Dalton Transactions

Accepted Manuscript

ROYAL SOCIETY OF CHEMISTRY

www.rsc.org/dalton

Cite this: DOI: 10.1039/c0xx00000x

www.rsc.org/xxxxxx

ARTICLE TYPE

Luminescent Metal-Organic Frameworks as Explosive Sensors

Debasis Banerjee, Zhichao Hu, and Jing Li*

Department of Chemistry and Chemical Biology, Rutgers University, Piscataway, NJ 08854

Received (in XXX, XXX) Xth XXXXXXXXX 20XX, Accepted Xth XXXXXXXXX 20XX
DOI: 10.1039/b000000x

Metal Organic Frameworks (MOFs) are of enormous current interest not only because of their fundamental importance but also due to their great potential for possible applications in gas storage and separation, catalysis, imaging and sensing, to name a few. Recent studies on luminescent MOFs (LMOFs) in both bulk and nanoparticle forms have shown that these materials possess excellent luminescence emission properties that may be utilized to effectively detect high explosive substances. Developing highly sensitive, selective, fast-responding and fully reversible sensor for the explosive detection is in great demand for the homeland security, environmental safety and other humanitarian concerns. In this perspective article, we discuss the development, possible mechanism and future aspects of explosive sensing by LMOF materials.

1. Introduction

Fast and efficient detection of high explosives is of current interest for a variety of reasons, including national security and environmental concerns.[1-10] [1] Nitroaromatic, nitroaliphatic and organic peroxide based compounds are generally used as the major ingredient of commercial explosives. For example, ammonal is an explosive composed of ammonium nitrate, trinitrotoluene (TNT) and aluminum powder. The ammonium nitrate works as an oxidizer for electron deficient TNT, while aluminum powder works as a fuel.[1] Plastic explosives are usually detected by sensing 2,3-dimethyl-2,3-dinitrobutane (DMNB), an added taggant as required by law in all commercial plastic explosives. The chemical structure of different nitroaromatic and nitroaliphatic based explosive molecules and their physical properties are listed in Fig.1 and Table 1 respectively. Various methods of explosive detection are currently available such as gas chromatography coupled with mass spectrometry,[11] surface enhanced Raman spectroscopy,[12] cyclic voltametry[13] and ion mobility spectrometry (IMS).[1] IMS instruments that are commonly used in airports have a detection sensitivity at ppb level, however they are expensive, not easily portable, prone to false positive and needs frequent calibration.[1] The use of trained canines is another common and effective way of detecting explosives, although they are labor intensive, costly, may not be always available, and not suitable for continuous monitoring.[1, 5]

Luminescent chemical sensors, such as conjugated polymers (CPs), have recently emerged as reliable alternatives for explosive detection.[4, 9, 14, 15] They are technologically friendly, easy to integrate to the existing infrastructure, have a low detection limit, and can selectively identify targeted molecules.

Table 1. The Vapor pressure and reduction potential of common explosives and selected analytes.

Analyte	Vapor Pressure (in mmHg,[#] at 25 °C)	Reduction Potential (in V *vs* SCE)
Nitrobenzene (NB)[16]	0.2416	-1.15
1,3-Dinitrobenzene (*m*-DNB)[17]	8.82 x 10^{-4}	-0.9
1,4-Dinitrobenzene (*p*-DNB)[16]	2.406 x 10^{-5}	-0.7
2-Nitrotoluene (NT)[16]	0.1602	-1.2
2,4-Dinitrotoluene (2,4-DNT)[16]	1.44 x 10^{-4}	-1.0
2,6-Dinitrotoluene (2,6-DNT)[16, 18]	5.61 x 10^{-4}	-1.0
2,3-Dimethyl-2,3-dinitrobutane (DMNB)[16, 18]	2.16 x 10^{-3}	-1.7
Benzene (BZ)[19, 20]	95.2	-3.42, -3.0
Toluene (TO)[21]	28.4	---
Ethylbenzene (Et-BZ)[22]	9.53	---
Cholorobenzene (ClBZ)[23, 24]	11.8	-3.2
Fluorobenzene(F-BZ)[25, 26]	70	-0.89
Nitromethane (NM)[26 24]	36.7	-0.160, -1.1
1-Nitroethane (NE)[24, 26]	15.6 (20°C)	-1.140
1-Nitropropane (NP)[26, 27]	7.5(20°C)	- 1.125
2,4,6-Trinitrotoluene (TNT) [16, 28]	8.02 x 10^{-6}	-0.7

1,3,5-Trinitroperhydro-1,3,5-triazine (RDX)[28]	4.6 x 10^{-9}	-0.79[29]
Ethylene glycol dinitrate (EGDN)[28]	2.8 x 10^{-2}	---
Trinitroglycerine (TNG)[28]	4.4 x 10^{-4}	---
Pentaerythritol tetranitrate (PETN)[28]	1.4 x 10^{-8}	---
Picric acid (PA) [28]	5.8 x 10^{-9}	-0.63[29]
Cyclotetramethylene tetranitramine (HMX)[28]	8.0 x 10^{-11}	-0.90[29]

[#] 1 mmHg = 1.2468 × 10^3 ppm

The detection process for these materials is primarily based on fluorescence quenching via donor-acceptor electron transfer mechanism (see Fig. 2).[1, 4, 9] For example, the presence of the delocalized π* excited state increases the electron donating ability of the polyacetylene,[30] metalloles[31] and phenyleneethynylene[16] based conjugated polymers, and therefore facilitates excitation migration process. This will significantly increase the electrostatic interactions between the polymeric aromatic moieties and enhance its further interaction with the explosive molecules. Similar electronic process is also observed in fluorescent molecular species where electron transfer is the dominant mechanism.[32]

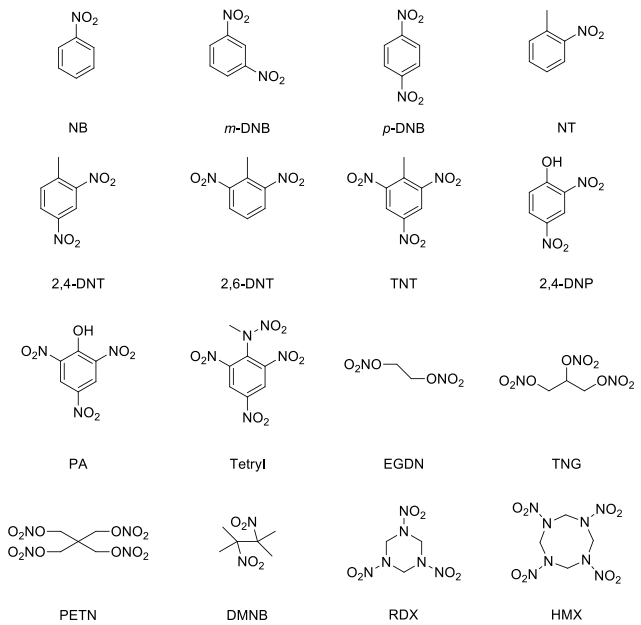

Fig.1. Chemical structures of common explosive and explosive-like molecules.[3, 7, 28]

Metal organic frameworks (MOFs) are a new class of crystalline materials. Many are porous with their pore diameters less than 1 nm. In these structures, metals or metal clusters are connected by organic ligands to form extended networks. They are promising for a broad range of applications, including gas storage and separation, catalysis, and sensing.[5, 6, 18, 33-45] The ability of luminescent MOFs (LMOFs) to propagate the host-guest interaction to detectable changes as a function of their luminescence makes them promising candidates for explosive sensing. LMOFs have several advantages over traditional conjugated polymers or molecular complexes, including simple one-pot and straightforward synthesis, and remarkable structural tailorability and functionalizability.[33] Furthermore, the combination of both inorganic and organic moieties within a single framework matrix allows systematic variation of fluorescent emissions by tuning different parameters such as metal ions, organic linkers or guest molecules. The adjustable pores, the immobilization of photoactive metal centers[33, 34] or highly conjugated organic linkers within the ordered framework can enhance the host-guest interaction by many folds.

The luminescence of LMOFs originates from a variety of sources such as metal centers, organic linkers, and charge-transfer processes such as ligand-to-metal charge transfer (LMCT), metal-to-ligand charge transfer (MLCT).[33, 34] The open channel structures and controllable pore sizes of LMOFs make them ideal candidates for guest-induced luminescence as well. As a result of such favorable properties, an increasing interest has been laid on LMOFs for their sensing applications. In this respect, the electronic properties of a given set of analytes (such as explosive molecules) and LMOFs are equally important for effective sensing. Quantitative evaluation of the efficiency of a particular LMOF sensor for a given analyte in liquid medium can be achieved using Stern-Volmer analysis (Eq. 1).[28, 46]

$$I_o/I_f = 1 + k_{sv}\cdot[Q] \quad (1)$$

In this formula I_o and I_f are the fluorescent intensities of the sensory material before and after the addition of the analyte, [Q] is the concentration of the analyte. and k_{sv} is the Stern-Volmer constant. The higher k_{sv} value indicates higher efficiency of the sensor. In this perspective, we discuss the development of different types of LMOFs on explosive detection and possible mechanisms involved in these processes.

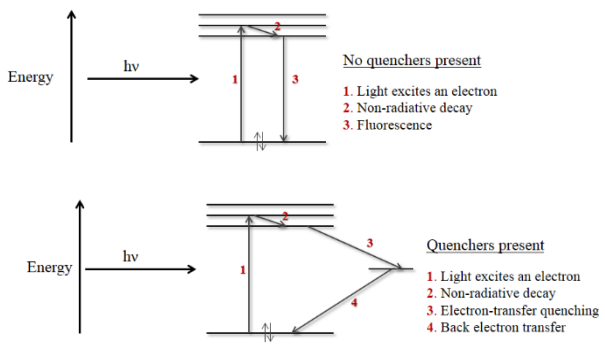

Fig. 2. Electron transfer mechanism of fluorescence quenching.[1]

2. LMOFs as Explosive Detectors

With the first work appeared only in 2009, LMOFs as explosive detectors represent a brand new sub-field of MOF research which remains little explored to date. Among the

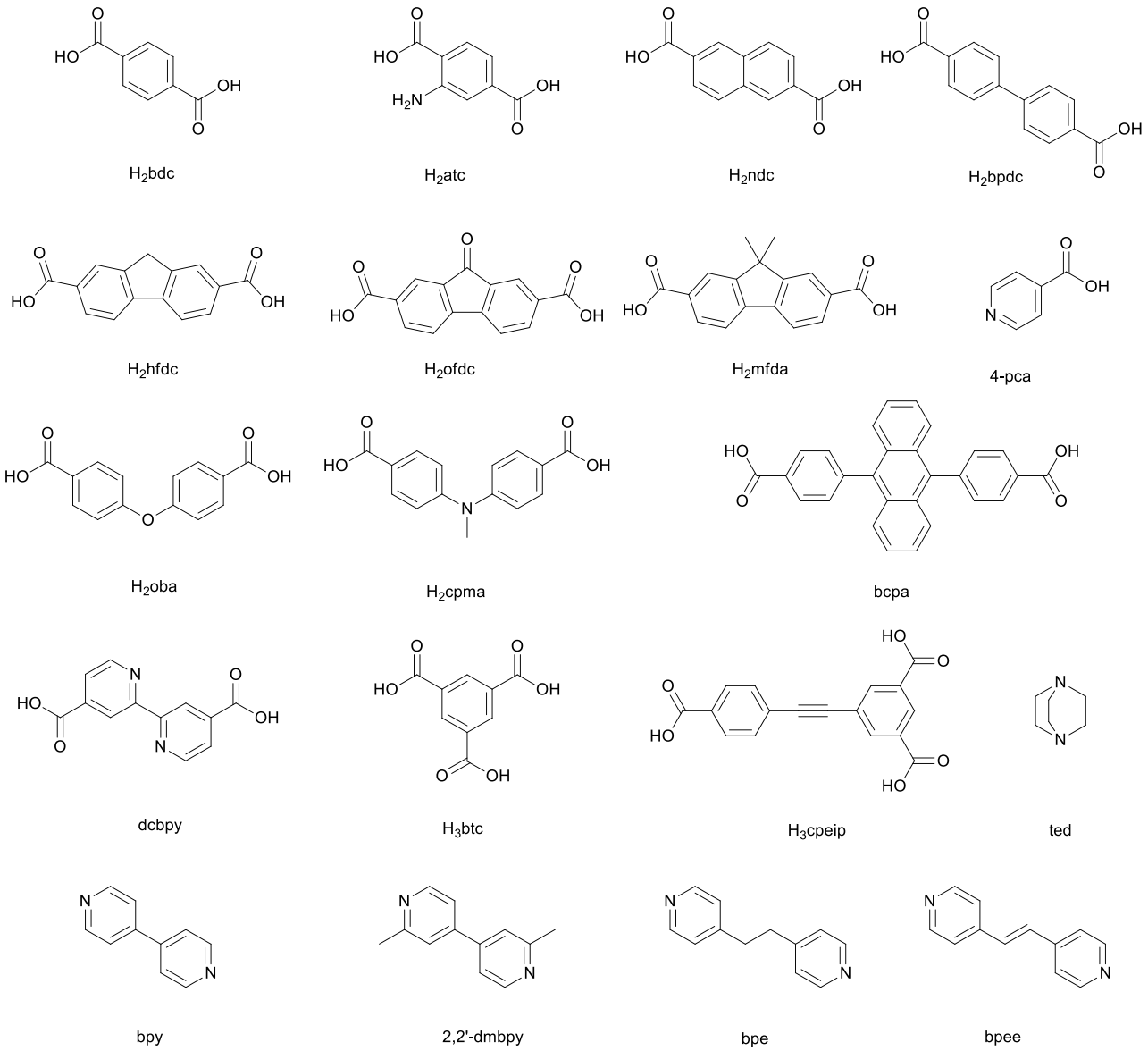

Fig. 3. Representative list of organic linkers used to construct various types of LMOFs (H_2bdc = 1,4-benzenedicarboxylic acid, H_2atc = 2-aminoterephthalic acid, H_2ndc = 2,6-naphthalenedicarboxylic acid, H_2bpdc = 4,4'- biphenyldicarboxylic acid, H_2hfdc = 9H-fluorene-2,7-dicarboxylic acid, H_2ofdc = 9-oxo-9H-fluorene-2,7-dicarboxylic acid, H_2mfda = 9,9- dimethylfluorene- 2,7-dicarboxylic acid, 4-pca = 4-pyridinecarboxylic acid, H_2oba =-4,4'-oxydibenzoic acid, H_2cpma = bis(4-carboxyphenyl)- N- methylamine, bcpa = 9,10-bis(p-carboxyphenyl) anthracene, dcbpy = 2,2′-bipyridine-4,4′-dicarboxylate, H_3btc = 1,3,5-benzenetricarboxylic acid, H_3cpeip = 5-(4-carboxyphenyl)ethynyl)isophthalic acid, ted = triethylenediamine, bpy = 4,4'-bipyridine, 2,2'-dmbpy = 2,2'-dimethyl-4,4'- bipyridine, bpe = 1,2-bis(4-pyridyl)ethane, bpee = 1,2-bis(4-pyridyl)ethylene).

reported studies, explosive sensing is investigated in both bulk and nanoparticle forms. The main difference between these systems lies in the kinetics of the analyte-MOF interactions. The small LMOF nanoparticles facilitate faster diffusion of the analyte molecules and thus show faster response. Representative examples of commonly used organic linkers and LMOFs investigated for explosive sensing are enlisted in Fig. 3 and Table 2, respectively.

2.1. Zinc Based LMOF Detectors

The luminescence in Zn-LMOF structures typically originates from emissive organic ligands. The ligand-based emissions are either from a single ligand or via a ligand-to-ligand charge transfer process. The formation of the 3D frameworks often enhance the ligand interactions and alter the HOMO-LUMO energy of the resultant structures, giving rise to different emission behaviors with respect to the molecular state. For example, changes in luminescence intensity and/or emission frequency.[23, 34, 43] We have reported the very first example of LMOFs as an efficient sensor for explosive detection.[5] LMOF-111 (or RPM3-Zn, a member of RPM series,[5, 18, 47-50] $Zn_2(bpdc)_2(bpee)\cdot 2DMF$, bpdc = 4,4'-biphenyldicarboxylate; bpee = 1,2-bis(4-pyridyl)ethylene) possesses a microporous framework with permanent and sustainable one-dimensional (1D) channels (see Fig 4). Its crystal

structure is composed of undulating neutral $[Zn_2(bpdc)_2]$ layers that are connected with each other by pillaring bpee ligands, forming a three dimensional (3D) network. The 1D open channels are along the crystallographic [010] direction with encapsulated solvent DMF molecules. The solvent DMF molecules can be readily removed upon heating or solvent exchange. The solvent removal leads to a structure change as indicated by the shift in the powder X-ray diffraction (PXRD) pattern. The outgassed framework shows permanent porosity with a Langmuir surface area of 483 m^2/g. Further, the outgassed sample reverts to the original form upon exposure to solvent DMF, characteristic of dynamic structural behavior. The outgassed sample shows strong solid-state luminescence at room temperature. Two analytes, representative of nitroaromatics and nitroaliphatics are selected to evaluate the detection performance of guest-free LMOF-111: DNT (0.18 ppm at 25 °C) for the former and DMNB (2.7 ppm at 25 °C) for the latter. The thin layer of solid samples shows rapid and reversible response to both types of vapor and within 10 seconds the quenching percentage [defined as $(I_o- I)/I_o \times 100\%$; I_o = original maximum peak intensity, I = maximum intensity after exposure] reaches the maximum (~85%) for both DNT and DMNB (see Fig. 5). The red shifts observed in the photoluminescence (PL) spectra of the outgassed sample upon exposure to the explosive vapors suggest strong interaction between the host framework and the analyte molecules. The PL of the sample can be recovered by heating at 150 °C for about a minute, and subsequent experiments show full recyclability (see insets in Fig. 5). The exceptional sensitivity and fast response of this framework towards the two analytes can be attributed to its 1D open channel which facilitate a strong confinement and fast diffusion of analyte molecules on the internal pore surface, and its extended 3D framework which enhances quenching via higher number of analyte binding sites within the channels. The effect of microporosity is evident from the fact that the as-synthesized sample (pores filled by solvent DMF molecules) gives a very poor quenching performance (ca. 8%) under the same experimental setting. The exceptional and record-making quenching response of the DMNB molecule (redox potential -1.7 V vs SCE; SCE = Saturated Calomel Electrode) is likely, at least in part, due to the high-lying conduction band (CB) and suitable pore size of this LMOF that lead to efficient electron transfer between the host and analyte. This study also demonstrates the effect of MOF particle size on the response time. Smaller particles (layer thickness ~5μ) can decrease the quenching time by 24 times with respect to larger particles (layer thickness ~ 30μ).

Our more recent study on another zinc based LMOF, LMOF-121 or $[Zn_2(oba)_2(bpy)]\cdot DMA$ (H_2oba = 4,4'-oxybis(benzoic acid), bpy = 4,4'-bipyridine, DMA = N, N'- dimethylacetamide) reveals interesting and new phenomena.[6] LMOF-121 is a porous structure built on $Zn_2(oba)_4$ paddle-wheel SBU (see Fig. 6a). Each SBU is linked by four oba ligands to form a distorted 4^4 net (see Fig. 6b). Two such identical nets interpenetrate to yield a 2D layered network (see Fig. 6c). The bpy ligands coordinate to the paddle-wheel units of the adjacent layers, generating a robust 3D framework with two intersecting 1D channels running

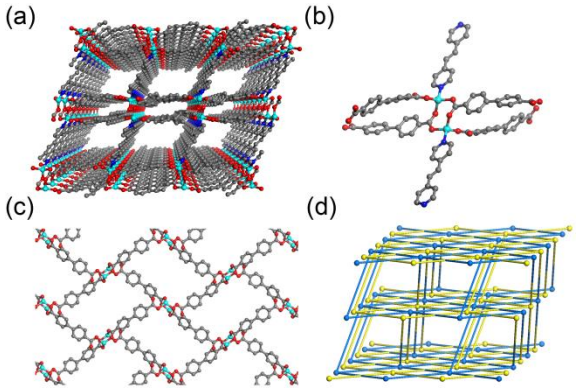

Fig. 4. a) Perspective view of the 3D structure of $[Zn_2(bpdc)_2(bpee)]$, showing the 1D channels along the *b* axis. b) The eight-membered ring-type SBU and the coordination around zinc metal centers. c) A single 4^4 net (Zn turquoise; C gray; O red; N blue). d) Simplified framework connectivity by linking the centroids of SBUs (spheres). Blue and yellow highlight the twofold interpenetration. Reprinted with permission from Ref. 5. Copyright 2009 Wiley-VCH.

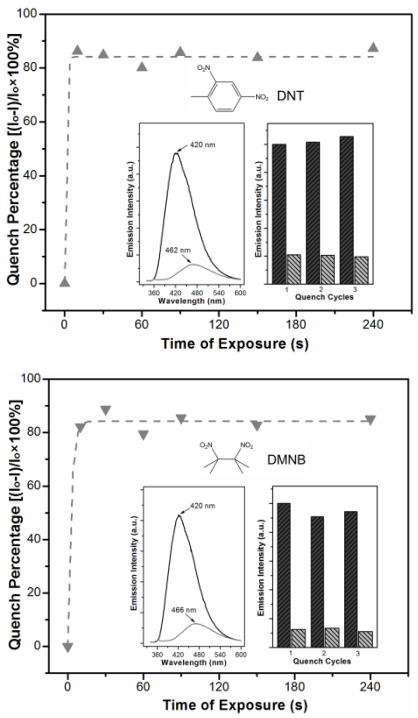

Fig. 5. Time-dependent fluorescence quenching profiles by a) DNT and b) DMNB. Insets: the corresponding fluorescence spectra before and after exposure to the analyte vapors for 10 s (left) and three consecutive quench/regeneration cycles (right). Reprinted with permission from. Ref. 5. Copyright 2009 Wiley-VCH.

along the crystallographic [100] and [010] directions. The average cross- sections of the channels are ~ 5.8 × 8.3 Å. The outgassed sample emits strongly (with a maximum at 420 nm) upon excitation at 280 nm. The compound shows opposite behavior when exposed to aromatic analytes with different electronic properties – group-A with electron withdrawing groups and group-B with electron donating groups. All nitroaromatic molecules act as a fluorescence quencher and the order of quenching effect is in accordance with their trend of electron withdrawing power and

vapor pressure (see Fig. 7a). For example, NB shows the highest quenching ability among all group-A members because of its high equilibrium vapor pressure and presence of an electron withdrawing $–NO_2$ group. The vapor pressure of NT is comparable with that NB, however the quenching level is much lower (29%) compared to NB because of the presence of electron donating $–CH_3$ group. On the other hand, analytes with more than one electron withdrawing groups such as *m*-DNB and *p*-DNB are less responsive, because of their low vapor pressure. All aromatic analytes with electron donating group (group-B members, Fig. 7b) show PL enhancement and the extent of such enhancement is consistent with their electron donating ability and vapor pressure. On the other hand, group-C analytes, those of nitroaliphatics such as DMNB, NM, NE and NP show negligible quenching effect for the outgassed sample, which is likely due to poor orbital overlap between the CB of the LMOF and the non-aromatic group-C analytes, as evident by density functional theory (DFT) calculations. The reduction potentials of the LMOF and the group-C analytes are also similar, lacking the driving force for any photoinduced electron transfer. In all scenarios, the PL of the host framework can be fully regenerated by heating the exposed sample at 150 °C for a few minutes.

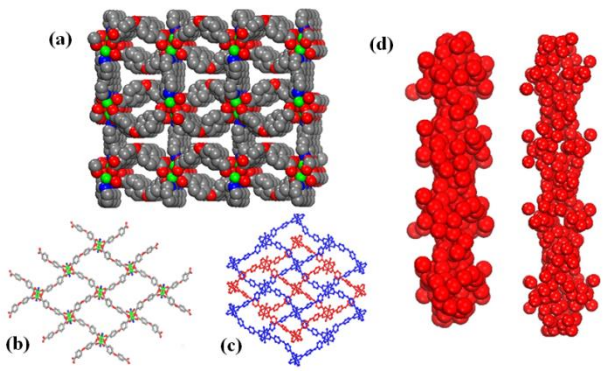

Fig. 6. Crystal structure of $[Zn_2(oba)_2(bpy)]\cdot DMA$ (a) Space-filling model of the 3D framework, showing the 1D channels running along the [100] axis (b) A single layer (Zn, green; O, red; N, blue). (c) Twofold interpenetration, shown by two different colors (blue and red). (d) He atom filling in a single channel along the (left) b and (right) [100] axes. Reprinted with permission from Ref. 6. Copyright 2011 American Chemical Society.

In addition, sensing behavior of a series of structurally related LMOFs of general formula Zn(L)(L')·G [L = ndc, L' = bpe (LMOF-161), bpee (LMOF-162), ted (LMOF-171), bpy (LMOF-181); ndc = 2,6- naphthalenedicarboxylate, bpe = 1,2-bis(4-pyridyl)ethane, ted = triethylenediamine, G = guest] have been investigated very recently. This group of MOF possesses jungle-gym type 3D frameworks made of zinc based paddle-wheel type secondary building units.[51] Each of the SBUs is bridged by dicarboxylate based ndc or bpdc ligands to form a 2D net which is further connected by different N-containing ligands (bpe, bpee, ted and bpy) as pillars to generate the overall 3D framework. The powder XRD analysis on the guest free samples shows that LMOF-181 remains highly crystalline upon removal of solvent molecules without any structural change. On the other hand, others undergo some structural changes as confirmed from their PXRD patterns. All the activated materials show PL quenching for groups-A analytes to various extent. Activated

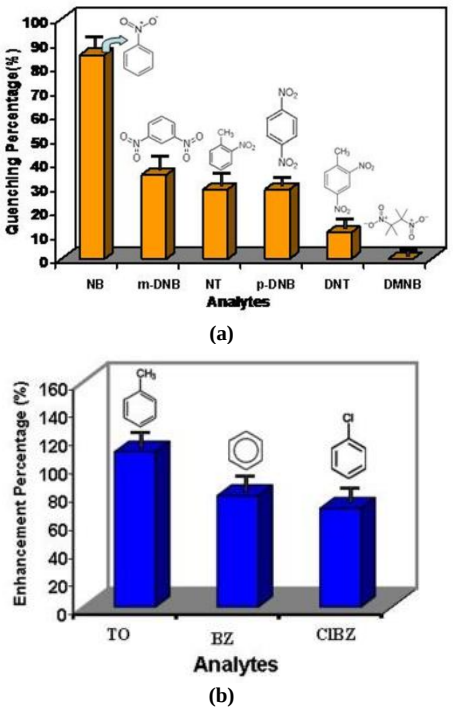

Fig. 7. (a) Percentage of fluorescence quench by five group-A aromatics. (b) Percentage of fluorescence enhancement of three group-B aromatics. Data are collected at room temperature at an exposure time of 15 mins. Reprinted with permission from Ref. 6. Copyright 2011 American Chemical Society.

LMOF-181 gives the best performance over other members of the series under similar experimental conditions, with about 84% and 51% quenching for vapors of NB and NT, respectively. They show PL enhancement upon exposure to group-B analytes and the trend roughly follows the order of vapor pressure and electron donating ability of the analytes. Group-C analytes such as NM and NP quench the PL of the activated materials, however to a significantly less degree compared to NB and NT, regardless of the fact that NM and NP have higher vapor pressures than the latter. This observation implies that aromatic molecules interact much more strongly with the LMOFs, as a result of strong π interactions between the analyte and aromatic pore surface of LMOFs and a more efficient electron transfer during the excitation process, which outweighs the effect of vapor pressure. NP shows a lower quenching efficiency between the two, as a result of the lower vapor pressure and larger molecular size of the NP compared to NM. The larger molecular size of an analyte leads to slower diffusion within the pore. The other group-C analyte, DMNB, does not have any effect on the photoluminescence properties of LMOFs studied due to its very low vapor pressure. The observed quenching/enhancement trend is not governed by a single factor but a number of variables including but not limited to the vapor pressure of the analytes, porosity of the LMOFs, relative orbital energies and electrochemical properties of the analytes and LMOFs, as well as the extent of their interactions.

A similar systematic study was recently carried out on a related LMOF system, namely $[Zn_3(bpdc)_3(bpy)]\cdot 4DMF\cdot H_2O$ (RPM1-Zn, LMOF-131),[47] $[Zn_3(bpdc)_3(2,2'\text{-dmbpy})]\cdot 4DMF\cdot H_2O$ (RPM7-Zn, LMOF-132),[49] $[Zn_2(bpdc)_2(bpe)]\cdot 2DMF$ (RPM4-Zn, LMOF-141)[50] and [Zn(bpdc)(bpe)]·DMF (RPM5-Zn, LMOF-

151) (2,2'-dmbpy = 2,2'-dimethyl-4,4'-bipyridine, DMF = N,N′-dimethylformamide, RPM = Rutgers recyclable porous material).[52] All four frameworks consist of the same metal center and dicarboxylate linker, but different N-containing linkers under different reaction conditions. The variation of synthesis conditions and N-based linkers lead to frameworks with different building units and topologies. Isostructural LMOF-131 and LMOF-132 possess a $Zn_3(COO)_6$ type SBU, with each SBU connecting six adjacent units via carboxylate groups of six bpdc linkers, forming a 2D double layer.. The overall framework is two-fold interpenetrated with 1D channel running along the crystallographic *b* axis. LMOF-141 is constructed of a dimeric $Zn_2(bpdc)_4$ type SBU, each of which is connected to four neighboring SBUs to form a 4^4 brick-like net. Two such identical nets interpenetrate to form a 2D double layer, which in turn connects to adjacent layers by N-containing bpe linker to form the overall 3D structure. LMOF-151 is composed of a five-fold interpenetrated 3D network, with tetrahedrally coordinated zinc metal centers, forming a primary building unit (PBU). Each of these PBUs is interconnected to generate the overall 3D diamondoid framework. All four frameworks remain crystalline after activation, although activated LMOF-141 and LMOF-151 show small shift of several peak positions, indicating structural changes upon removal of the guest molecules. The guest dependent fluorescence properties were tested using members of group-A & group-B analytes at room temperature. The results show that all nitroaromatics (group-A) act as florescence quencher, with a general order of quenching efficiency NB > NT > DNB > DNT, which can be explained by factoring the vapor pressure and electron withdrawing ability of the analytes. Group-B analytes act as fluorescence enhancer similar to other LMOFs materials with the enhancement efficiency related to the vapor pressure and electron donating ability of the analytes. Interestingly, LMOF-141 also shows frequency shift when exposed to group-B analytes, which provides an additional variable for the identification of different analytes in the same category. The extent of fluorescence intensity change roughly follows the order of their porosity. For example, activated LMOF-131 exhibits significantly higher extent of both quenching and enhancement in comparison with LMOF-151, a less porous member of the group, while the two have very similar electronic properties. Electrochemical measurement and theoretical calculation further reveal that the MOF-analyte interaction follows similar mechanistic pathway as described in case of other LMOFs: electron deficient (rich) analytes quench (enhance) the PL of LMOFs. Subsequently, we developed a new strategy utilizing the emission frequency shift of LMOF based sensors.[23] LMOF-161 and 162 $[Zn_2(ndc)_2(L)]\cdot G$ [L= bpe, bpee] are closely related structures constructed on a $Zn_2(ndc)_4$ paddle-wheel SBU. The SBU connects to four identical units to form 2D net. The net is further bridged by the pillar (bpe, bpee) linkers to form a 3D network. Two of such networks interpenetrate to give rise to the overall structure (see Fig. 8, top). Both frameworks exhibit structural change upon activation, likely due to the absence of specific interaction between the two interpenetrated frameworks. Both materials show fluorescence quenching for group-A analytes and enhancement for group-B analytes. Additionally both show emission shift upon exposure to various analytes. Emission frequency (wavelength) shift generally results from strong analyte-LMOF interactions, e.g. formation of an exciplex during excitation. Such shift in wavelength upon contact with different analytes is particularly effective in distinguishing analytes with similar electronic properties such as different nitroaromatics (see Fig. 8, middle). The incorporation of frequency shift parameter adds a new dimension to the conventional analyte detection based on fluorescence intensity change and can be a powerful tool in effectively identifying and differentiating analytes on a two-dimensional basis. For example, both DMNB and RDX show very similar quenching profile towards LMOF-162, but have different frequency shift, enabling a clear distinction between the two. As such, all the explosives (TNT, RDX), taggant (DMNB) and analytes of groups-A, -B and -C can be uniquely identified on the 2D map (see Fig. 8, bottom). A surfactant [hexadecyl-trimethyl-ammonium bromide (CTAB)] assisted synthesis was further employed to reduce the particle size of the compounds to 1-5 μm, as compared to 50-120 μm sized particle found in solvothermally synthesized bulk samples. The observed response time in achieving a certain emission shift shortens by 4-5 times for a given analyte as a result of particle size reduction. *In-situ* IR (Infrared) adsorption spectroscopy was employed to study and characterize the interaction between selected analytes, NB and NT from group A and BZ and TO from group B with the LMOF-162. The red shift of the υ_{19} band in adsorbed BZ and TO analyte suggest weakening of the phenyl bonds, possibly due to withdrawal of electron density from the phenyl ring π orbital, as a result of LMOF-analyte interaction. On the other hand the stretching bands of the electron withdrawing $-NO_2$ group, υ_{as} and υ_s in adsorbed NB and NT show significant red shifts, indicating electron-density redistribution from LMOF to the adsorbed analytes. Further, both molecular dynamics and ab initio based theoretical calculations were carried out on the LMOF-162 using two selected analytes (NB and NM). The strong interaction between the lowest unoccupied molecular orbital (LUMO) of the analytes and the CB of the LMOF leads to slight change in the CB energies, leading to a small increase in the band gap, therefore a blue shift in the emission. The interaction is stronger for NM than for NB, and as a result, a larger blue shift is observed for NM than NB.

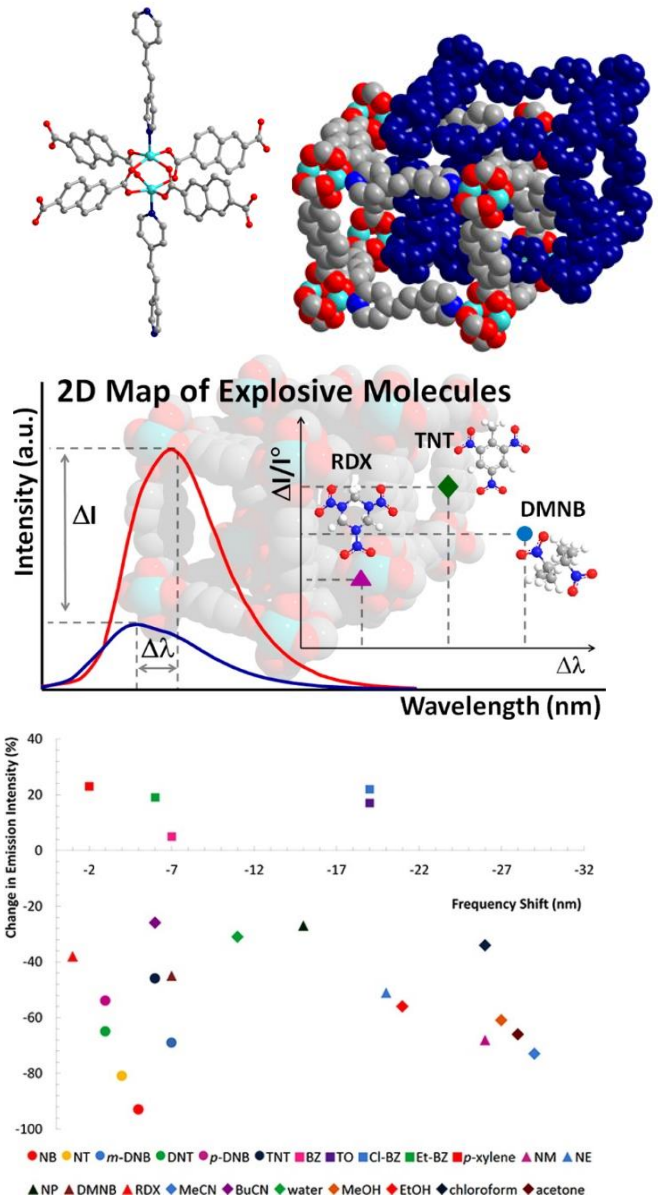

Fig. 8. Top: Crystal structure illustration of $[Zn_2(ndc)_2P$, *P* = bpe or bpee.(LMOF-161 & 162) Middle: An illustration of the analyte-induced two dimensional responses (Δλ and ΔI). and the generation of a 2D map. Bottom: A 2D color-coded map of analyte recognition by LMOF-162. Reprinted with permission from Ref 23. Copyright 2013 American Chemical Society.

An alternate strategy for detecting high explosives having extremely low vapor pressure such as RDX and HMX is to detect the volatile components in these plastic explosives, such as solvents, stabilizers, and plasticizers. This strategy was applied for rapid and selective detection of cyclohexanone, a solvent used in the recrystallization of RDX and coexisting in the product mixture, by using LMOF-202, $[Zn_2(hdfc)_2(bpy)\cdot xDMA$, hfdc = 9H-fluorene-2,7-dicarboxylate].[53] The emission intensity of the activated LMOF-202 was enhanced after 10 second of exposure to various ketones, with varying degree of emission shifts for different ketones. Thus each ketone can be pin-pointed on a 2D map using both parameters. Molecular orbital calculation shows that the high-lying LUMO orbitals of the ketones facilitate the electron transfer to the CB of host framework. Furthermore, the large spectral overlap found between the absorbance of host and the emission of the ketones allows for effective energy transfer between the two, therefore increasing the emission enhancement. On the contrary, activated LMOF-121, a LMOF with similar porosity and electronic properties as activated LMOF-202, shows a significantly lower percentage of PL enhancements under same experimental conditions, which is due to decreased spectral overlap between the analytes and the host framework. Such observations further confirm that energy transfer plays an equally important role in fluorescence response. Similar observation was noticed for group-A analyte, DNT, through emission quenching for both LMOF-121 and -202. Notably, the K_{sv} of LMOF-121 is 2.3 times of that of LMOF-202, which is most likely due to the spectral overlap between the absorbance of DNT and the emission of LMOF-121, while such overlap is nearly negligible for LMOF-121. This particular observation once again confirms energy transfer as a predominant factor for emission response. Another closely related structure, namely, LMOF-201 $(Zn_2(ofdc)_2(bpy)\cdot 2.5DMF\cdot 1.25H_2O$, ofdc = 9-oxo-9H-fluorene-2,7-dicarboxylate) has similar electronic properties as LMOF-202, but shows no change in emission intensity upon exposure to ketone vapors because of it nearly nonporous nature. These results indicate that porosity and electronic properties of host frameworks are important parameters for sensing ketone analytes, similar to what was observed for group-A, -B, and -C analytes.

Recently, Ghosh and coworkers[54] reported a LMOF, $[Zn_{1.5}(L)(H_2O)]$ [L = $H_3(C_{27}H_{16}O_6)$, a flexible tripodal organic linker], composed of bilayer sheets of the tripodal organic linkers, connected by the linear trimeric zinc clusters at each end, forming a 2D sheet with hexagonal pores of ~ 12.2 × 13.4 Å dimension. The aromatic moieties are involved in π -π stacking interaction within each layer and between adjacent 2D sheets. The activated material shows strong solid-state fluorescence at 390 nm upon excitation at 280 nm at room temperature. Moreover the activated material shows emission quenching for group-A and -C analytes by means of solid state vapor sensing. NB shows the highest amount of quenching (~86% after 10 min exposure) followed by NM (75%), NT (66%), DMNB (57%), 2,4-DNT (53%), 2,6-DNT (46%) and NP (39%). The observed trend can be explained based on a combination of factors including vapor pressure, electron withdrawing ability and electronic properties of the analytes and the supramolecular wire effect imposed by the host framework. For example, electrostatic potential plot (ESP) shows that 2,4-DNT has a better chance of interacting with electron rich π system of the activated material due to favorable orientation. The improved quenching efficiency of nitroaliphatic analyte DMNB that lacks any conjugated π system, is explained by the orbital overlap between the electron rich π system of the host LMOF and the electron deficient $-NO_2$ groups of the analyte. The supramolecular wire effect, involving a long range migration of excitons facilitates such an overlap. For smaller group-C analytes such as NM the observed quenching might be influenced by steric effect; as NM can access the interlayer space readily over bulkier analytes such as NP.

Qian, Chen and coworkers have reported sensing ability of $[Zn_4(OH)_2(1,2,4\text{-btc})_2(H_2O)_2]\cdot 0.63DEF\cdot 3.5H_2O$ (btc = 1,3,5-

benzenetricarboxylate, DEF = N, N'- diethylformamide) on selected nitroaromatics (including DNT and TNT) in solution phase.[55] The 3D framework contains 1D channels of a cross section of ~ 6.2 × 5.7 Å along the crystallographic [100] axis. The free and coordinated solvent molecules present in the channels can be removed by thermal activation. The permanent porosity of the desolvated material is confirmed by gas adsorption experiment, which gives a BET surface area and pore volume of 408 m^2/g and 0.205 cm^3/g, respectively. The crystal structure of the activated material remains intact upon activation as evident from the PXRD analysis. The methanolic solution of the activated compound shows strong quenching effect to nitrobenzene molecules. The inclusion of the analytes is confirmed by IR spectra of the samples after nitrobenzene soaking. The authors attributed the quenching to the charge transfer effect from the aromatic linkers of the LMOF to the electron deficient guest molecules as well as π -π interaction between the host framework and analyte molecules.

Using a dicarboxyl functionalized schiff base linker *L* (H_4L = 1,2-phenylendiamine-N,N′-bis(3-tert-butyl-5-(carboxyl)-salicylide-ene), Cui and coworkers[56] have synthesized two Zn-containing LMOF structures, $[Zn_4O(ZnL)_3(DMSO)_5]\cdot 3DMSO\cdot 5H2O$ and $[Zn_2O(ZnL)_2(bpy)(DMA)(H_2O)]\cdot 4DMA\cdot 4H_2O$ (DMSO = dimethyl sufoxide). Both frameworks form neutral 3D net with large parallelogram channels along crystallographic [010] direction. The metal centers are present in either distorted tetrahedral or octahedral coordination, based on the ligand environment. The frameworks retain structural integrity upon solvent removal as confirmed by the PXRD and gas adsorption measurements. The presence of Zn(salen) based structural unit, previously used in sensing applications in molecular form makes it natural to anticipate similar properties in the extended structures.[32] Indeed both the activated frameworks emit strongly at 525 and 535 nm, respectively, when excited at 420 nm. Further, both frameworks show PL quenching response upon exposure to different nitroaromatic vapors including NB and two NT isomers. Nitrobenzene shows the highest quenching ability owing to its high vapor pressure and presence of strong electron withdrawing $–NO_2$ group. The quenching performance is dependent on the exposure time and is recorded up to 44% and 67% for the two frameworks, respectively, at 10 seconds. The higher quenching level of one of the frameworks is attributed to its larger open channels, allowing the explosive analyte molecules to diffuse inside the channels and interact with the zinc metal centers more effectively.

Sun and coworkers reported two zinc based LMOFs $Zn_3(L1)_2(L_2)\cdot 3.6DMF\cdot 4.0H_2O$ and $Zn_3(L_1)2(L_2)$ [L_1 = 4-[3-(4-carboxyphenoxy)-2-[(4-carboxyphenoxy)methyl]-2-methyl-propoxy]benzoate, L_2 = 1,4-bis(1-imidazolyl)benzene] forming 3D framework with trimettalic structural building blocks under different synthetic conditions.[57] The first one has a two-fold interpenetrating framework with guest solvent molecules in the channel while the later forms a dense three-fold interpenetrated framework. The different degrees of interpenetration within the two different frameworks leads to different level of interactions between the organic linkers, affecting the ligand centered luminescence emission. The porous two-fold interpenetrated framework was further activated and its luminescence behavior was measured along with the as-synthesized dense framework. Both of them emit upon excitation at 246 nm, with the emission band maximum at 326 and 392 nm, respectively. The luminescent properties of both LMOFs were further studied by dispersing these materials in different solvents such as DMF, methanol, acetone, chloroform, dichloromethane, tetrahydrofuran, acetonitrile, BZ, TO, and NB. The PL spectra are dependent on the solvents particularly for DMF and NB, which exhibit the strongest enhancing and quenching behavior, respectively. The dense framework based emulsion shows higher sensitivity towards NB solution than the activated porous framework, reaching up to ~98% quenching at 50 ppm concentration. The high quenching caused by NB for both compounds is attributed to the electron transfer from excited state of the electron donating MOF framework to electron withdrawing NB molecules. Another factor for such a high selectivity is the highly dispersible nature of the MOF particles in the DMF solvent, leading to enhanced contact between the MOF particle and the analyte.

2.2. Cadmium Based LMOF Detectors

In addition to zinc containing LMOFs, several cadmium based LMOFs have also been investigated for their explosive detection performance. Cadmium and zinc are members of same row in the periodic table and as a result have similar physical properties. However one major disadvantage for any practical applications of cadmium based LMOFs is the toxicity involving cadmium. However, they can well be used as a model system for understanding aspects of explosive sensing. Indeed, an interesting paper regarding the explosive sensing mechanism was reported by Ghosh and coworkers[58] using a luminescent MOF, $[Cd(ndc)_{0.5}(pca)]$ (pca = 4-pyridinecarboxylic acid), which can selectively detect TNP (2,4,6-trinitrophenol or picric acid: PA) over other group-A analytes (see Fig. 9, top). The compound possesses 1D channel along crystallographic *c* axis. The cross section of the channel is ~ 9.48 × 7.83 Å, and the channel wall is decorated by the π electron rich aromatic rings and Lewis basic pyridine nitrogen atom. The structural integrity of the materials holds upon activation as evident from PXRD, CO_2 and benzene sorption analysis. The activated material, dispersed in acetonitrile shows strong emission at 384 nm and moderate emission at 470 nm, when excited at 340 nm. The acetonitrile dispersed activated material shows fast and high fluorescence quenching upon addition of TNP solution (~78% upon addition of 1mM solution, see Fig. 9 middle), while little quenching effect was observed for other group-A and group-C analytes such as TNT, 2,4-DNT, 2,6-DNT, DNB, NB, DMNB and NM. The Stern-Volmer (SV) plot of TNP is nonlinear at higher concentration, in contrast to other group-A and group-C analytes under similar conditions, indicative of a different mechanism of emission quenching for TNP than a common photoinduced electron transfer (PET) mechanism. The quenching constant for TNP is $3.5 \times 10^4\ M^{-1}$, which is ~ 30 times greater than for TNT. Furthermore, the addition of aqueous solution of TNP (1 mM) to the activated material (in acetonitrile) leads to similar fluorescence quenching response (~78%). Quenching response for TNP remains unaffected even in presence of other

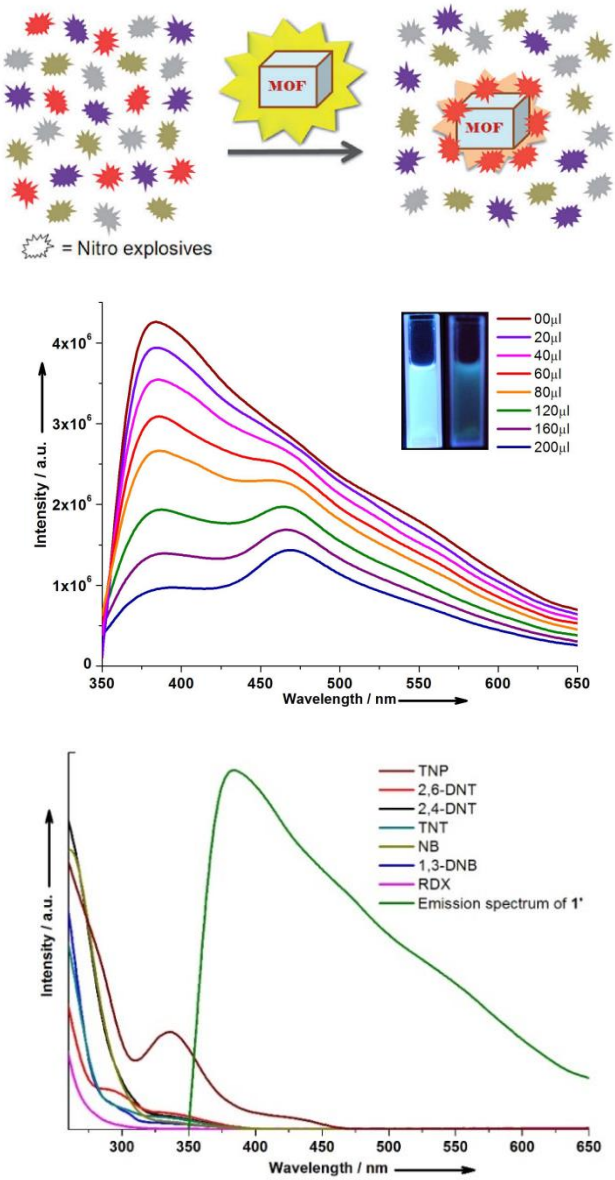

Fig. 9. Top: An illustration of an LMOF-based sensor, $[Cd(ndc)_{0.5}(pca)]$, for the selective detection of targeted nitro explosive in the presence of other nitro compounds. Middle: Effect on the emission spectra of the activated LMOF dispersed in acetonitrile upon incremental additional of a TNP solution. The inset photograph shows the original florescence and the decreased fluorescence upon additional of TNP. Bottom: Spectral overlap between the absorption spectra of analytes and the emission spectrum of the LMOF (green solid line). Reprinted with permission from ref. 58. Copyright 2013 Wiley-VCH.

group-A analytes. The selectivity of the activated material towards TNP is attributed to electron and energy transfer mechanisms, as well as electrostatic interactions between the analyte and the Lewis basic site. A resonance energy transfer between the host and a group-A analyte occurs when there is a spectral overlap between the adsorption band of the analyte and the emission band of the host material. Such an overlap increases the quenching efficiency and sensitivity for a particular analyte depending on the extent of spectral overlap. In the current case, the absorption band of TNP shows the largest spectral overlap with the emission band of activated material, consistent with the observed strongest quenching effect over other group-A analytes (see Fig. 9, bottom). The energy transfer is a long range process and therefore the emission quenching by TNP is carried over by surrounding aromatic moiety or fluorophores, amplifying the quenching response. PET on the other hand is a short range process where the analyte molecules only interact with fluorophores in direct contact and as a result the emission quenching is not as pronounced. The presence of the dominating energy transfer was also supported by the preferential quenching of the 384 nm peak over 470 nm. The peak at 384 nm has a spectra overlap with the absorption spectrum of TNP, and as a result efficient quenching of the peak occurs by an energy transfer mechanism. On the contrary, the 470 nm peak has no overlap with the adsorption spectrum of TNP and as a result the quenching occurs by a 'less efficient' PET process, leading to lesser quenching. Furthermore, the material remains selective due to the presence of free pyridyl nitrogen group on the pore surface help boosting TNP selectivity for the activated material, by means of electrostatic interaction between hydroxyl group of the analyte and Lewis basic pyridyl nitrogen. The postulate was further backed up by fluorescence quenching titration and the acidity order of the analytes.

Liang and coauthors[59] reported another cadmium based LMOF sensor, $[Cd(cpeip)_2(DMF)_3]$, composed of neutral non-oxo triangular $[Cd_3(COO)_6]$ SBU and a rigid unsymmetrical tricarboxylate ligand H_3cpeip [H_3cpeip = 5-(4-carboxyphenyl)ethynyl)isophthalic acid]. The ethanolic suspension of micrometer sized MOF particle shows strong luminescence emission at 417 nm, when excited at 342 nm. Moreover, it shows significant quenching for PA (~84.2% for 91.3 μM PA solution) over other group-A analytes such as 2,4-DNT, 2,4-dinitrochlorobenzene (2,4-DNCB), 4-chloronitrobenzene (4-NCB) and 4-nitrobenzaldehyde (4-NBA). The emission spectra further exhibit a red shift upon addition of PA solution, indicating strong interaction between the LMOF and PA. In general, the practical use of cadmium based LMOFs will be limited compared to the zinc based LMOFs. Nevertheless, cadmium LMOFs with unique topologies and sensing properties are worth of fundamental studies.

2.3. Main Group Metal Based LMOF Detectors

The research related to main group metal based MOFs for explosive sensing is quite sporadic. The luminiscence observed in these compounds generally originates from the oragnic linkers via intra- or inter-ligand charge tranfer process.[60] Recently, Moon and coworkers[60] reported a LMOF, $\{Li_3[Li(DMF)_2](cpma)_2 \cdot 4DMF \cdot H_2O$ [H_2cpma = bis(4-carboxyphenyl)- N-methylamine] for detecting nitroaromatic based explosives. The SBU in this structure is a 1D chain made of tetrahedrally coordinated LiO_4. Each chain is bridged with four neighboring chains by dicarboxylate ligands, in four different directions. Such an atomic arrangement leads to a 3D network with two kinds of rectangular channels, along the *c* axis. The channels are filled with free and coordinated DMF molecules, respectively. The activated LMOF changes to a different structure with a total loss of porosity as evident by the PXRD and N_2 adsorption data. The as-synthesized material was tested as a detector for analytes such as NB, 2,4-DNT, BZ and TO in liquid state A concentrated DMF solution of 2,4-DNT was used for the detection, whereas all other analytes were used as is. A drastic color change from pale yellow to red or deep orange was observed, when immersed in NB

and DNT analyte respectively. In contrast, it retains original color upon soaking in BZ and TO. The origin of such color change in NB was investigated using single crystal X-ray diffraction method along with IR and elemental analysis. The single crystal data reveal that NB is easily adsorbed inside the channel as a guest molecule due to the strong π−π interactions with the aromatic pore surface. The single crystal data also indicate strong interaction between the guest $-NO_2$ group and the linker π system. Furthermore the presence of bulky NB group in the channel induces intra-ligand motion, leading to stronger C−H···π interactions in the framework. Such intra-ligand motion could have drastic effect on the electronic structure of the material itself.

The UV/Vis absorption spectrum of as-synthesized material in the solid state shows two absorption peaks, at 248 and 352 nm, with appearance of an additional absorption peak at around 500 nm. The intense red color of the NB soaked material is attributed to the charge-transfer between the aromatic rings of the electron-rich linker and the electron-deficient NB. The material can be regenerated by heating under vacuum at 100 °C for 5 minutes. The as-synthesized LMOF exhibits intense fluorescence at λ_{max} = 430 nm when it is excited at 345 nm as a result of strong ILCT (Intraligand charge transfer) from the donor N-methylamino group to the acceptor carboxylate groups within the linker. On the other hand, NB soaked as-synthesized material is completely non-emissive under excitation at 345 nm. Similar behavior is observed for DNT (in DMF solution) soaked material, which can be explained as a result of electron transfer donor-acceptor mechanism via host-guest interaction.

Chen and coworkers[61] reported a microporous, anionic LMOF $[In_2L_3][NH_2(CH_3)_2]_2(DMF)_4(H2O)_{16}$ [L = tetrakis[(3,5-dicarboxyphenoxy methyl]methane], which shows sensing properties for group-A and -B analytes. The framework is composed of tetrahedrally connected indium metal center and eight connected organic linker, forming an anionic, open framework with interconnecting channels along crystallographic a, b and c direction. The as-synthesized LMOF emits strongly at 360 nm upon excitation at 280 nm at room temperature, exhibiting a blue shift with respect to the free ligand (420 nm). The material show typical fluorescence quenching for group-A analyte in liquid and vapor phases. The quenching order roughly follows the order of electron withdrawing ability and size of the analytes. The fluorescence quenching response to different analyte was attributed to the electrostatic interactions between the anionic framework and the electron-deficient nitroaromatic analytes and pore confinement of the analyte inside the channel.

2.4. Metal-Organic Gel (MOG) Based Detectors

Metal Organic Gels (MOGs) is an important sub-class of MOFs, with possible applications in catalysis and selective gas-separation. Structurally, they can be described as materials with high internal surface area and without any long range order.[62] Conjugated polymers based on triptycene core exhibit interesting sensing phenomenon towards different explosives via fluorescence quenching mechanism.[9, 63] Recently Berke and coworkers[64] used a triptycene based polycarboxylic acid to form metal organic gel (MOG) material, incorporating aluminum metal center. Dynamic rheology experiments confirmed the gel-like character of the synthesized material. The dispersed gel in ethanol emits strongly at 385 nm upon excitation at 318 nm, which is red shifted by 10 nm in comparison to the peak at 375 nm for the free linker when excited at 315 nm. The interaction of the gel (dispersed in ethanol) with different analytes was monitored by fluorescence quenching experiments. The quenching response varies upon addition of analytes with different electron deficiency. The ethanol dispersed gel exhibits efficient quenching for hydroxy substituted nitroarene such as p-nitrophenol (p-NP), 2,4-DNP, 2,6-DNP and PA. It shows the highest sensitivity for PA (in the range of 5-10 ppb) among all the analytes selected. The quenching efficiency of the gel was further evaluated using Stern-Volmer equation. The quenching constant for PA ($K_{sv} = 5.3 \times 10^5\ M^{-1}$) was found to be 3 times higher than the binding constant of the same analyte for the free linker. The increased quenching response for the gel is attributed to the formation of the self-assembly of the triptycene receptors in a porous structure to facilitate long range exciton migration.

The ethanol dispersed gel can be recovered by centrifugation and washing, showing retention of the emission intensity up to 75% after six cycles, demonstrating the high photostability of the material. The performance of the gel to sense different analytes in solid state was also evaluated using different nitroaromatics such as NB, 2,4-DNT and PA. The sensing performance however is much less pronounced in the solid state. For example, the material exhibits a significant quenching (55%) of the initial intensity upon exposure to NB vapor for 6 min, while only 13% and 9% quenching is observed for 2,4-DNT and PA, respectively. The trend of quenching response is in contrast with that observed in liquid state, but in accordance with the increasing vapor pressure of the analytes. In addition to Al-based MOG, the Co-based 3D MOF $[Co_2(ttc)(DMF)(H_2O)$ [ttc = 1,4,5,8-triptycene tetracarboxylate) and the Cr-based MOG synthesized using the same organic linker were also tested for sensing of PA. Both of them show lower sensitivity with respect to the Al-MOG, as calculated by Stern-Volmer equation. However, no rational was given due to lack of structural information of the MOG materials.

2.5 Lanthanide Based LMOF Detectors

Lanthanide metal ions are unique as they luminesce when excited at a particular wavelength. The weak light adsorption by the lanthanide ions because of forbidden f-f transition, however, make the direct excitation of the ions highly inefficient. The introduction of light absorbing organic linker to form a lanthanide based LMOF leads to strong intramolecular interaction between the metal center and the organic linker, commonly known as 'antenna effect', which greatly enhance the optical performance of the LMOFs.[34, 43] Several groups have reported explosive detection using lanthanide based LMOFs. For example, Xiao and coworkers reported the synthesis of highly luminescent nanocrystals of a terbium-based LMOF, [Tb(1,3,5-btc)]n (btc = benzenetricarboxylate) using a combined ultrasound-vapor phase diffusion technique. The compound displayed strong solid-state luminescence at 491, 546, and 589 nm upon excitation at 324 nm at room temperature. Interestingly, the nano-sized material shows high sensitivity toward PA in solution phase (> 75% luminescence quenching at 90 ppm), however no obvious quenching effect was observed towards the nitroaromatic analytes including NB, 2-NT, 2,4-DNT, 2,6-DNT and common organic solvents such as acetone and acetonitrile. The high selectivity and sensitivity were attributed to the strong supramolecular interactions (e.g. hydrogen bonding) between the framework and the PA molecules, which

may facilitate the charge transfer between the analyte and the framework, in addition to the common electron-transfer donor–acceptor mechanism, resulting in a much higher quenching efficiency.

Zhou and coworkers reported a microporous 3D LMOF $Eu_3(mfda)_4(NO_3)(DMF)_3$ [H_2mfda = 9,9-dimethylfluorene- 2,7-dicarboxylic acid], with 1D channel of rhombic-shaped cross section and pcu structure topology.[65] Both as-synthesized compound and its activated form are highly luminescent and exhibit characteristic Eu(III) emission profile. The activated form shows luminescence quenching in solution state for group-A analytes, among which3,4-DNT is found to be the most effective quencher with a quenching efficiency of ~ 45% (0.5 mM conc. solution in DMF). An emission enhancement was also observed for group-B analytes such as TO. To understand the quenching mechanism further, the luminescence lifetime of the activated material was measured at different concentrations of 1,2-DNB. The similar lifetime in each concentration of the analyte suggests an absence of interaction between the analytes and the metal center.[65] Thus changes in emission intensity are related to the interactions between the analytes and the organic linker. The quenching trend of group-A analytes was further attributed to a combination of factors including molar absorption coefficient (ε) and electron withdrawing abilities of the analytes. A larger molar absorption coefficient (ε) means higher light energy absorption for the analytes, which leads to lower light absorption for the linker itself. Since the PL properties of the host framework originates as a result of absorption of energy by the mfda linker and the vibronic coupling between the linker and the metal center, this leads to an overall emission quenching. A similar structure, $\{[Eu_2(mfda)_2(HCOO)_2(H_2O)_6]\cdot H_2O\}n$ was reported successively by the same group. [66] The activated material shows selective detection of PA with a detection limit of around ~10^{-7} M in DMF solution. Additionally, the active material show moderate luminescence quenching for other group-A analytes such as 2,6-DNT, 2,4-DNT, 2-NT and 1,3-DNB. The higher quenching sensitivity of PA is due to the hydrogen-bonding interactions between the carboxylate groups of organic linker and hydroxyl groups of PA.

2.6. Nanoparticle Based LMOF Detectors

In addition to the development of LMOF detectors in bulk form (macroscopic particles), a considerable effort is being made on LMOFs in form of nanoparticles for improved performance in explosive detection, as the sensing kinetics may be substantially enhanced with smaller particle sizes. The initial work has been made on the nanocrystalline forms of known MOF structures. One such example is the synthesis and PL study of a europium based nano-MOF, $[Eu_2(bdc)_3(H_2O)_2]\cdot(H_2O)_2$ (H_2bdc = 1,4-benzenedicarboxylic acid), which is isostructural to a previously reported terbium-benzenedicarboxylate framework (see Fig. 10a).[67] The nano-MOF crystals of rod shape with diameters less than 20 nm show typical fluorescence emission characteristic of lanthanides while dispersed in ethanol solution (see Fig. 10b-c). Addition of various nitrobenzene based analytes to the solution (e.g. a concentration of ~ 150 ppm for 2,4-DNT and TNT) leads to a significant quench of the PL intensity when excited at 315 nm (see Fig. 10d). The inclusion of group- B molecules such as benzene, phenol and toluene on the other hand does not affect the PL intensity. This is very different from what have been observed in the case of $[Zn_2(oba)_2(bpy)]$ (LMOF-121).[6]The luminescence lifetime of the nano-MOF remains unaffected upon addition of analytes at different concentration, indicating absence of any electronic interaction between the metal center and the analyte. The quenching trend of group-A analytes were attributed to the light absorption efficiency of respective analytes similar to the one described above for $Eu_3(mfda)_4(NO_3)(DMF)_3$.[65] For example, group-A analytes such as NB, 2,4-DNT and TNT shows strong absorbance at 315 nm due to π -π^* transition, decreasing the energy transfer from bdc to the metal center. The reduction in energy transfer leads to effective emission quenching.[67]

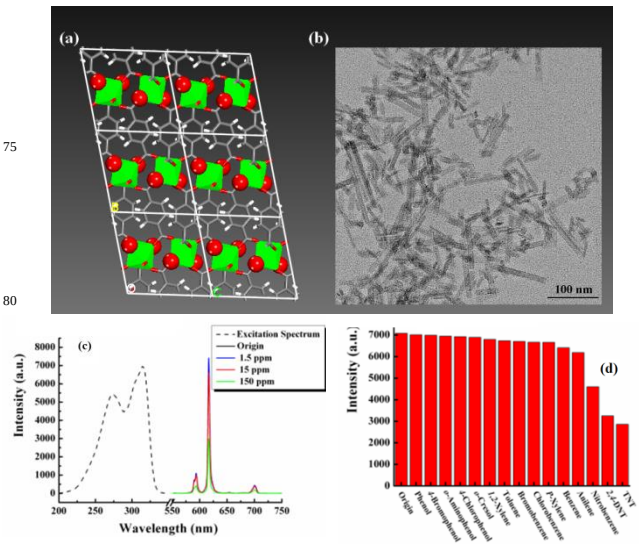

Fig. 10. (a) Structure of $[Eu_2(bdc)_3(H_2O)_2]\cdot(H_2O)_2$ viewed along the [100]-axis (Eu, green; C, gray; H, white; O, red; water molecules, red balls) (b) TEM image of nanorods. (c) Excitation and emission spectra of the unexposed LMOF, and LMOF exposed to TNT solutions at different concentrations (1.5, 15, 150 ppm). (d) the PL emission intensities of the $^5D^0$-$^7F^2$ transition in ethanol solution of the MOF nanorods with 150 ppm of different analytes (excited and monitored at 315 and 617 nm, respectively). Reprinted with permission from Ref. 67. Copyright 2009 Royal Society of Chemistry.

Employing a similar strategy, Qiu and coworkers have carried out a surfactant assisted synthesis and solution-based photoluminescence study of a layered lanthanide nano-MOF, $[Eu_2(bdc)_3(H_2O)_2]$ with an average particle diameter of 200 nm.[68] The emission intensity of the material in acetonitrile solvent changes significantly upon exposure to various nitroaromatic based explosive molecules such as 2-NT (nitrotoluene), 4-NT, 2,4-DNT, 2,6-DNT (200 µL to 2 ml acetonitrile solution of dispersed nano-MOF) similar to other fluorescent nano-MOFs. Among numerous nano-MOFs of d^{10} metal centers that have been investigated for their sensing properties toward explosive detection are Zn(bcpa) (bcpa = 9,10-bis(p-carboxyphenyl) anthracene[69] and $[Zn_4O(L_4)_2(H_2O)_3]\cdot 3DMA\cdot 3EtOH\cdot 6H_2O$ (H_3L_4 = 5-(4-carboxyphenylethynyl) isophthalic acid).[70] For Zn(bcpa), the nanocrystalline nature of the particles ranging between 500 nm and 1µm forbids full structural elucidation and thus energy dispersive X-ray (EDX) spectroscopic method was used to identify zinc,

oxygen and carbon in the material, with the PXRD confirms long range ordering. The fluorescence properties of the material arise due to the presence of highly conjugated organic linker bcpa, making it a good choice for sensory applications. A drop-cast thin film of the material was exposed to saturated vapor of various nitroaromatic explosive such as DNT and TNT at different time interval. The exposure of DNT to the thin film leads to 62% quenching within 10 seconds and reaches 80% at equilibrium. The material demonstrates slower sensitivity towards TNT compared to DNT because of the low volatility of TNT. Despite the weak oxidizing nature of nitroaliphatic species which translates to weak electron affinity, the material shows high level of sensitivity towards NM vapor. Depending on its vapor concentration, the PL quenching varies from 21% at 360 ppm level to almost 100% with a 100 fold increase in vapor concentration. The sensitivity in PL quenching is attributed to the large surface-to-volume ratio and stronger analyte binding efficiency in the MOF structure, which is further supported by the poor PL quenching efficiency of the free linker. In the case of $Zn_4O(L_4)_2(H_2O)_3$, a similar study is performed on nanocrystals made of highly π-conjugated linker L_4. The material consists of a Zn_4 cluster based SBU, each of which is connected by the organic linkers to form a 3D framework. Such connectivity leads to the formation of 1D open channel with a cross-section of ~ 14.2 × 13. 5 Å along crystallographic [010] axis. The micrometer sized particles of the compound shows intense PL emission at 470 nm upon excitation at 350 nm. The ethanol dispersed nanoscale crystals shows further enhanced sensitivity towards ethanolic solutions of different nitroaromatic molecules such as DNT and TNT. The high sensitivity towards TNT is particularly noteworthy, reaching up to ppb (parts per billion) level which is lower than the permissible level in drinking water as established by EPA (Environmental Protection Agency). Interestingly, the PL intensity is unperturbed in presence of various nitroalkanes and aromatic molecules. This observation is similar to what has been reported earlier on $Zn_2(oba)_2(bpy)$,[6] which is most likely due to the comparable redox capability of the MOF and analytes, hindering an effective electron transfer in the excited state. The exposed nanocrystals can be recycled by simple centrifuging and washing with ethanol.

The detection of explosive vapors by nano-MOFs was also studied by Qiu and coworkers,[71] using a MOF nanotube (MOFNT) material based on a known cadmium based MOF of general formula $[Cd_2(btc)_2(H_2O)_2]$.[72] The MOFNT was obtained using 'self-sacrificing' template strategy, the MOF nanorods were formed first under the applied synthetic conditions, followed by formation of nanotubular particles, by the dissolution of the nanorods. The nanotubes with inner diameters of 50–150 nm and outer diameters of 100–300 nm were structurally characterized by PXRD, energy-dispersive X-ray (EDX) spectroscopy, transmission electron microscopy (TEM) and elemental analysis. The MOFNTs show strong solid-state fluorescence at 406 nm, upon excitation at 315 nm at room temperature. The effect of different nitroaromatics such as NB, 2-nitrotoluene (2-NT), 4-nitrotoluene (4-NT) and DNT on the fluorescence properties were investigated using fluorescence spectrometric titration experiment, revealing strong quenching phenomenon, while no quenching effect was observed for non-nitro compounds including toluene (TO), benzene (BZ), chloroform, acetonitrile, DMF, dimethyl sulfoxide (DMSO), and tetrahydrofuran (THF). In particular, MOFNTs show strong response to DNT vapor, reaching a quenching value of 72.5% within 10 s after the sample was placed in DNT-saturated vapor. This performance is better than most fluorescence-based chemical sensing materials,[16, 73] and close to previously reported $Zn_2(bpdc)_2(bpee)$.[5]

Similar work on cadmium and zinc based nano-MOFs were reported by Wen and Qiu, respectively.[74, 75] The cadmium based nano-MOF $[Cd(atc)(H_2O)_2]_n$ (H_2atc = 2-aminoterephthalic acid) was synthesized using co-precipitation method with the formation of nanorods of 20-40 nm thickness and widths of 80-100 nm.[74] The nano-MOF has the same 1D zigzag chain motifs as the bulk structure as confirmed by PXRD.[76] Each of these chains is further involved in noncovalent interactions to form a 3D network structure. The nano-MOF dispersed in ethanol shows photoluminescence at 434 nm, upon excitation at 340 nm as a result of intra-ligand emission. The fluorescence intensity of the material decreases significantly upon addition of 2 ml of 0.2 M ethanol solution of different nitroaromatics such as NB, 2-NT, 3-NT and 4-NT. The order of quenching efficiency matches well with the order of electron withdrawing effect (NB > 4-NT > 3-NT) of the analytes. The addition of other aromatic analytes such as TO, bromobenzene (Br-BZ), and iodobenzene (I-BZ) have no effect on the fluorescence properties of the material.

The zinc benzenedicarboxylate (bdc) based nano-MOF was synthesized using a surfactant CTAB assisted technique and was characterized by a variety of physical measurements such as PXRD, scanning electron microscopy (SEM) and TEM.[75] The nano-MOF has a similar topology as the bulk layered $Zn(bdc)\cdot xH_2O$ [x = 1-2] as evident from the PXRD patterns.[77] Nanosheets with width of 50-100 nm, length of 200-500 nm, and thickness of 50-80 nm were obtained first, which converted to nanorods over time (180-360 min) in the mother liquor. The nanorods so formed show blue solid state fluorescence at 427 nm, upon excitation at 304 nm, due to LMCT process. Further, the material dispersed in acetonitrile shows fluorescence quenching in presence of 9.76×10^{-2} M nitrobenzene solution of different volume (0.2 -1 µM). As expected, the quenching increases with increasing amount of nitrobenzene.

2.7. Heterobimetallic MOF Based Detectors

The incorporation of prefabricated luminescent molecular complex within a rigid framework offers a range of benefits including predictable optical properties and enhanced thermal stability, beneficial for selective explosive sensing. Luo and coworkers[78] reported a heterobimetallic MOF, $[ZnL_2]\cdot3DMF\cdot5H_2O$ [L = $[Ir(ppy)_2(dcbpy)]$, ppy = 2-phenylpyridine, dcbpy = 2,2′-bipyridine-4,4′-dicarboxylate] based on a prefabricated photoactive iridium complex. Iridium based molecular complexes are able to achieve sensitization in the visible spectrum and have relatively long luminescent lifetimes. The solid state emission spectrum of the free iridium complex shows a strong emission band at 575 nm, while the MOF fluoresces with an emission maximum at 602 nm, indicating the fluorescence of the later is generated by the prefabricated complex. The red shift was attributed to the immobilization of the prefabricated molecular complex within the framework and its coordination with the zinc metal center. Methanol dispersed microcrystals of the compound

shows distinct liquid state emission which is quenched by group-A analytes. The order of quenching at the same concentration is TNT > DNT ≈ p- DNB ≈ m-DNB > NB. For example, TNT shows a detectable emission quenching at ppm scale with quenching efficiency reaching 70% at a concentration of 625 ppm. The same group[79] successively reported an anionic photoluminescent heterobimetallic MOF, $[InRu(dcbpy)_3][(CH_3)_2NH_2]\cdot 6H_2O$, using similar prefabrication strategy by using prefabricated $[Ru(H_2dcbpy)_3]^{2+}$ metalloligand moiety. The MOF exhibits a broad absorption band (250 - 650 nm) and strong red light emission with long decay lifetime, originating from metal to ligand charge transfer process within the metalloligand. The free metalloligand display strong solid state red photoluminescence at 633 nm upon excitation at 400 nm, while the framework exhibit a fluorescence maximum at 657 nm upon excitation at the same wavelength. The similar shape and energy maxima of the emission bands of the two indicate that the fluorescence of the framework originates from the metalloligand itself. The red shift is attributed to the coordination of metalloligands with the metal centers, similar to the earlier report.[79] The emission intensity of the framework material does not change for non-nitro analytes such as BZ, TO and phenol in liquid state upon soaking a thin layer of the as-synthesized material in their respective methanolic solution, however the fluorescence emission quenching was observed for group-A analytes under similar conditions. TNT shows the highest quenching efficiency (25% at 125 ppm concentration) among the entire group-A analytes investigated, followed by other group-A analytes under similar experimental condition. The fluorescence quenching in both cases was attributed to a photoinduced electron transfer between analyte and the host framework.

2.8. Simulation Work

The molecular simulation studies so far have been limited in evaluating MOFs as pre-concentrator of explosive molecules,[80-82] because MOFs can selectively adsorb appreciable amount of common explosive molecules. The pre-concentrator step is essential for improved sensitivity of existing sensory materials. The presence of ordered, tunable pores in MOFs makes them better candidates for selective adsorption of various molecules including explosives, and for increased sensitivity as a result of confinement. Several IRMOFs (Iso-reticular MOFs) have been evaluated for their pre-concentration capabilities of high explosive RDX using computational methods, including classical molecular dynamics (MD) and Grand Canonical Monte Carlo (GCMC) simulation. The IRMOFs were selected because of their high porosity and proven gas-diffusion capability. Moreover, their isostructural character makes them an ideal system to compare the effect of pore size and functional groups on the pre-concentration ability of the MOF materials. The calculations provide useful information on the diffusion process of RDX molecules in the activated materials at room temperature and at low RDX concentration.[80, 81] IRMOFs possess either large or small cages within the framework, depending on the orientation of the organic linkers. The simulation studies on various IRMOFs (notably IRMOF-1, -3, -8, -10) reveal that the steric hindrance by the organic linkers plays an important role in the adsorption capacity as well adsorption mechanism of the explosive molecules.[80, 81] The adsorption occurs on the material surface and/or interior large cages and the extent depends on the steric effect of the linker. The RDX molecules interact strongly with the Zn_4O based connector sites in case of surface adsorption, while they interact more strongly with the aromatic linkers in the interior where the steric hindrance from the linkers prevents connector-RDX interactions. The presence of amine functionalized linkers increases the adsorption of the RDX molecules as they offer more interaction sites. However the higher amine-analyte interaction energy may hinder the practical applications of IRMOFs as preconcentrator because of the difficulty in desorption process. The evidence of surface adsorption suggests that preconcentrator efficiency might be tuned by varying IRMOF particle size.

2.9. Possible Mechanisms

As previously mentioned, the fluorescence emission in LMOFs may originate from a variety of sources, including metal centers, conjugated linkers, charge transfer between metals and linkers or between different linkers. The mechanism of fluorescence based sensing may follow an electron transfer or energy transfer process, or a combination of the two, which may lead to a change in emission intensity or a shift in emission wavelength, or a combination of both. A short-ranged electron transfer can lead to fluorescence quench or enhancement of the host framework. Similar physical processes have long been studied in conjugated polymer based sensors which are attributed to the photoinduced donor-acceptor electron transfer from the host to the guest analyte molecules (see Fig. 2). While extensive studies have been conducted on conjugated polymer and metal complex based sensors to investigate and understand quenching mechanism, only a few are reported for MOF based sensors to date. [23, 51, 52] A detailed electronic band structure calculation on LMOF-121 suggests that the PL quenching process may follow the same donor-acceptor electron transfer mechanism for the conjugated polymers.[6] For group-A analytes the lowest unoccupied molecular orbital (LUMO) is a low-lying π^*-type orbital and its energy is below the conduction band (CB) minimum of the host framework. This allows electron transfer from the LMOF to the analyte upon photoexcitation, leading to fluorescence quenching. For analytes having electron donating groups (group-B), the LUMO is a high-lying π^* antibonding orbital with the energy above the CB of the host framework and therefore the electron transfer leads to fluorescence enhancement. Consistent explanations may be attained based on the reduction potentials of the LMOFs and analytes. The cyclic voltammetry study shows that group-A analytes have more positive reduction potential, while group-B analytes have more negative potential,

Table.2. Selected list of LMOFs, excitation and emission wavelengths, sensing techniques and targeted explosive molecules.

Metal	LMOF	λ_{ex} (nm)	λ_{em} (nm)	Sensing Technique	Molecules	Ref.
Li	$\{Li_3[Li(DMF)_2](cpma)_2\}\cdot 4DMF\cdot H_2O$	345	430	Liquid	Nitroaromatic	[60]
Zn	$[Zn_2(oba)_2(bpy)]\cdot DMA$ [LMOF -121]	280	420	Vapor	Nitroaromatic & Nitroaliphatic	[6]
	$[Zn_3(bpdc)_3(bpy)]\cdot 4DMF\cdot H_2O$ [LMOF-131]	300	420	Vapor	Nitroaromatic	[52]
	$Zn_2(bpdc)_2(bpee)\cdot 2DMF$ [LMOF-111]	300NS	420	Vapor	Nitroaromatic & Nitroaliphatic	[5]
	$[Zn(ndc)(bpy)_{0.5}]$ [LMOF-181]	300	450	Vapor	Nitroaromatic & Nitroaliphatic	[51]
	$Zn(bdc)\cdot xH_2O$ [x = 1-2]	304	427	Liquid	Nitroaromatic	[75]
	$[Zn_3(bpdc)_3(2,2'\text{-dmbpy})]\cdot 4DMF\cdot H_2O$ [LMOF-132]	320	388	Vapor	Nitroaromatic	[52]
	[Zn(bpdc)(bpe)]·DMF [LMOF-151]	330	425	Vapor	Nitroaromatic	[52]
	$[Zn(ndc)(bpe)_{0.5}]$ [LMOF-161]	330	425	Vapor	Nitroaromatic & Nitroaliphatic	[51]
	$[Zn_2(bpdc)_2(bpe)]\cdot 2DMF$ [LMOF-141]	330	450	Vapor	Nitroaromatic	[52]
	$[Zn(ndc)(bpee)_{0.5}$ [LMOF-162]	330	450	Vapor	Nitroaromatic & Nitroaliphatic	[51]
	$[Zn_4(OH)_2(1,2,4\text{-btc})_2(H_2O)_2]\cdot 0.63DEF\cdot 3.5H_2O$	331	428	Liquid	Nitroaromatic	[55]
	$[Zn(ndc)(ted)_{0.5}]$ [LMOF-171]	340	420	Vapor	Nitroaromatic & Nitroaliphatic	[51]
Cd	$[Cd_2(btc)_2(H_2O)_2]$.	315	406	Liquid	Nitroaromatic	[71]
	$[Cd(ndc)_{0.5}(pca)]$	340	384(s), 470 (m)	Liquid	Nitroaromatic	[58]
	$[Cd(atc)(H_2O)_2]_n$	340	434	Liquid	Nitroaromatic	[74]
	$[Cd(cpeip)_2(DMF)_3]$	342	417	Liquid	Nitroaromatic	[59]
In	$[In_2L_3][NH_2(CH_3)_2]_2(DMF)_4(H_2O)_{16}$	280	360	Liquid/Vapor	Nitroaromatic	[61]
Ln	$Eu_3(mfda)_4(NO_3)(DMF)_3$	336	581, 592, 615	Liquid	Nitroaromatic	[65]
	$[Eu_2(bdc)_3(H_2O)_2]\cdot(H_2O)_2$	315	590, 617, 698	Liquid	Nitroaromatic	[67]
	$[Tb(1,3,5\text{-btc})]_n$	324	491, 546, 589	Liquid	Nitroaromatic	[83]
Zn-Ir	$[ZnL_2]\cdot 3DMF\cdot 5H_2O$ [L = $[Ir(ppy)_2(dcbpy)]$	-	602	Liquid	Nitroaromatic	[78]
In-Ru	$[InRu(dcbpy)_3][(CH_3)_2NH_2]\cdot 6H_2O$	400	657	Liquid	Nitroaromatic	[79]

NS = Not Specified

with respect to the host framework. As a result, the host framework acts as an electron donor in the case of group-A analytes, and as an electron acceptor in the case of group-B analytes upon excitation. The effect of group-C analytes, including nitroalkanes such as NM, NE, and 1-NP may vary, depending on, at least partially, their electron donating/withdrawing ability relative to that of the LMOFs, while short ranged

photoinduced electron transfer is often a dominating mechanism for fluorescence based detection by LMOFs, mechanisms such as

long-range energy transfer also plays a key role in such processes. A necessary condition of such energy transfer is the overlap between the emission spectrum of an LMOF and the absorption spectrum of an analyte or vice versa. Being a long range process, the quenching effect of the analyte is not limited to one fluorophore, but carried over to multiple adjacent fluorophore (e.g. aromatic moiety), enhancing the overall effect.[53, 58] Emission frequency shift of the host LMOF may result from strong LMOF-analyte interaction such as formation of an exciplex during excitation process.[84 85, 86] The process is often specific for a particular set of analyte and LMOF system. As LMOFs with different topology and composition have different energy levels, the extent of their interactions with different analytes will vary.

3. Summary and Future Prospect

The usefulness of LMOFs for possible sensing related applications largely depends on their performance in selective and specific molecular recognition. The ability of MOFs for surface functionalization via either pre- or post- synthetic modification techniques gives them competitive edge for utility in these applications. In this perspective, we show that LMOFs are promising candidates for detection of various explosive molecules by monitoring changes in their optical emissions. Several classes of LMOFs have already been shown to have excellent reversibility, selectivity and sensitivity towards targeted explosives. The majority of the research so far has been focused on bulk LMOFs, but with an increased attention on nano-MOFs. Another detection strategy relies of the use of prefabricated photoactive molecular complex to form heterobimetallic LMOFs. The immobilization of photoactive molecular complex with an extended framework is particularly helpful for designing new optical sensors with designated properties. Current work involving different types and forms of LMOFs, as well as a large class of explosive or explosive-like molecules provides timely information and insight on the topic. For practical applications, however, the ideal candidates need to demonstrate exceptional selectivity, fast response, high sensitivity, and full recyclability.

Finally, the study of LMOFs for explosive detection represents a relatively new research area and is still in its infancy. Only a very small percentage of such materials have been evaluated so far, given the immense structural diversity of this class of compounds. By deliberately tuning their crystal structures, composition and porosity, optimal electronic structures, optical emission and redox properties may be achieved to enhance and improve their detection performance.

Acknowledgements

This work is supported by Department of Energy (DOE) through Grant No. DE-FG02-08ER46491.

Corresponding Author

Address: Department of Chemistry and Chemical Biology Rutgers University, Piscataway, NJ 08854, USA. Fax: 732-445-5312; Tel: 732-445-3758; E-mail: jingli@rutgers.edu

List of Abbreviations

1D	one-dimensional
2,2'-dmbpy	2,2’-dimethyl-4,4’bipyridine
2,4-DNT	2,4-dinitrotoluene
2,4-DNP	2,4-dinitrophenol
2,4-DNCB	2,4-dinitrochlorobenzene
2,6-DNT	2,6-dinitrotoluene
2D	two-dimensional
2-NT	2-nitrotoluene
3D	three-dimensional
3-NT	3-nitrotoluene
4-NT	4-nitrotoluene
4-NCB	4-chloronitrobenzene
4-NBA	4-nitrobenzaldehyde
H_2atc	2-aminoterephthalic acid
H_2bdc	1,4-benzenedicarboxylic acid (also terephthalic acid)
H_2bpdc	4,4'-biphenyldicarboxylic acid
bpca	9,10-bis(p-carboxyphenyl) anthracene
bpdc	4,4’-biphenyldicarboxylate
bpe	1,2-bis(4-pyridyl)ethane
bpee	1,2-bis(4-pyridyl)ethylene
bpy	4,4'-bipyridine
Br-BZ	bromobenzene
H_3btc	1,3,5-benzenetricarboxylic acid
BZ	benzene
CB	conduction band
CL-20	Hexanitrohexaazaisowurtzitane
CL-BZ	chlorobenzene
Cpeip	5-(4-carboxyphenyl)ethynyl)isophthalic acid
H_2cpma	bis(4-carboxyphenyl)- N-methylamine
CTAB	hexadecyl-trimethyl-ammonium bromide
dabco	1,4-diazabicyclo[2.2.2]octane (also ted: triethylenediamine)
dcbpy	2,2′-bipyridine-4,4′-dicarboxylate
DEF	N,N-diethylformamide
H_2hdfc	9H-fluorene-2,7-dicarboxylic acid
DFT	density functional theory
EPA	Environmental Protection Agency
ILCT	Intraligand charge transfer
H_4L	1,2-phenylendiamine-N,N′-bis(3-tert-butyl-5-(carboxyl)-salicylide-ene
L_1	4-[3-(4-carboxyphenoxy)-2-[(4-carboxyphenoxy)methyl]-2-methyl-propoxy]benzoate
L_2	1,4-bis(1-imidazolyl)benzene
L_3	tetrakis[(3,5-dicarboxyphenoxy methyl]methane
H_3L_4	5-(4-carboxyphenylethynyl) isophthalic acid
LUMO	Lowest Unoccupied Molecular Orbital
DMA	N,N'-dimethylacetamide
H_2mfda	9,9-dimethylfluorene- 2,7-dicarboxylic acid
DMF	N,N-dimethylformamide
DMNB	2,3-dimethyl-2,3-dinitrobutane
DMSO	Dimethyl sulfoxide
ESP	electrostatic potential plot
FBZ	fluorobenzene
m-DNB	1,3-dinitrobenzene
p-DNB	1,4-dinitrobenzene
DNT	dinitrotoluene
EGDN	ethylene glycol dinitrate
Et-BZ	ethylbenzene
V	electron volts
G	guest
GCMC	grand canonical Monte Carlo
HMX	octahydro-1,3,5,7-tetranitro-1,3,5,7-tetrazocine
I-BZ	iodobenzne
IMS	ion mobility spectrometry

IR	Infrared
IRMOFs	Isoreticular MOFs
LMCT	ligand-to-metal charge transfer
LMOFs	luminescent metal-organic frameworks
MD	molecular dynamics
MLCT	metal-to-ligand charge transfer
MOFs	metal-organic frameworks
MOFNT	MOF nanotube
MOG	metal organic gel
NB	nitrobenzene
H_2ndc	2,6-naphthalenedicarboxylic acid
ndc	2,6- naphthalenedicarboxylate
NE	nitroethane
NM	nitromethane
NP	1-nitropropane
NT	2-nitrotoluene
H_2oba	4,4'-oxydibenzoic acid
oba	4,4'-oxydibenzoate
H_2ofdc	9-oxo-9H-fluorene-2,7-dicarboxylic acid
ONC	octanitrocubane
p-NP	p-nitrophenol
PA	picric acid (also TNP: 2,4,6-trinitrophenol)
PBU	primary building unit
PETN	pentaerythritol tetranitrate
PET	photo induced electron transfer
PL	photoluminescence
ppy	2-phenylpyridine
PXRD	powder X-ray diffraction
RDX	1,3,5-trinitroperhydro-1,3,5-triazine
RPM	Rutgers recyclable porous material
SBU	secondary building unit
SCE	Saturated Calomel Electrode
SEM	scanning electron microscopy
SV	Stern - Volmer
ted	triethylenediamine (also dabco: 1,4-diazabicyclo[2.2.2]octane)
TEM	transmission electron microscopy
Tetryl	2,4,6-trinitrophenylmethylnitramine
TGA	thermogravimetric analysis
TNG	trinitroglycerin (also NG: nitroglycerin)
TNP	2,4,6-trinitrophenol (also PA: picric acid)
TNT	2,4,6-trinitrotoluene
TO	toluene
ttc	1,4,5, 8-triptycene tetracarboxylate
XRD	X-ray diffraction

References:

1. S. J. Toal and W. C. Trogler, *J. Mat. Chem.*, 2006, **16**, 2871-83.
2. L. Senesac and T. G. Thundat, *Mat. Today*, 2008, **11**, 28-36.
3. Y. Salinas, R. Martinez-Manez, M. D. Marcos, F. Sancenon, A. M. Costero, M. Parra and S. Gil, *Chem. Soc. Rev.*, 2012, **41**, 1261-96.
4. D. T. McQuade, A. E. Pullen and T. M. Swager, *Chem. Rev.*, 2000, **100**, 2537-74.
5. A. J. Lan, K. H. Li, H. H. Wu, D. H. Olson, T. J. Emge, W. Ki, M. C. Hong and J. Li, *Angew. Chem. Int. Ed.*, 2009, **48**, 2334-38.
6. S. Pramanik, C. Zheng, X. Zhang, T. J. Emge and J. Li, *J. Am. Chem. Soc.*, 2011, **133**, 4153-55.
7. M. E. Germain and M. J. Knapp, *Chem. Soc. Rev.*, 2009, **38**, 2543.
8. D. S. Moore, *Rev. Sci. Intrum.*, 2004, **75**, 2499-512.
9. S. W. Thomas, G. D. Joly and T. M. Swager, *Chem. Rev.*, 2007, **107**, 1339-86.
10. B. Liu, *J. Mat. Chem.*, 2012, **22**, 10094-101.
11. K. Hakansson, R. V. Coorey, R. A. Zubarev, V. L. Talrose and P. Hakansson, *J. Mass Spectrom.*, 2000, **35**, 337-46.
12. J. M. Sylvia, J. A. Janni, J. D. Klein and K. M. Spencer, *Anal. Chem.*, 2000, **72**, 5834-40.
13. M. Krausa and K. Schorb, *Journal of Electroanalytical Chemistry*, 1999, **461**, 10-13.
14. S. W. Thomas, J. P. Amara, R. E. Bjork and T. M. Swager, *Chem. Comm.*, 2005, 4572-74.
15. H. R. Nie, Y. Zhao, M. Zhang, Y. G. Ma, M. Baumgarten and K. Mullen, *Chem. Comm.*, 2011, **47**, 1234-36.
16. J. S. Yang and T. M. Swager, *J. Am. Chem. Soc.*, 1998, **120**, 11864-73.
17. R. Hoffmann, *J. Chem. Phys.*, 1963, **39**, 1397-412.
18. A. J. Lan, K. H. Li, H. H. Wu, L. Z. Kong, N. Nijem, D. H. Olson, T. J. Emge, Y. J. Chabal, D. C. Langreth, M. C. Hong and J. Li, *Inorg. Chem.*, 2009, **48**, 7165-73.
19. J. Mortensen and J. Heinze, *Angew. Chem. Int. Ed.*, 1984, **23**, 84-85.
20. http://www.epa.gov/ttn/atw/hlthef/benzene.html.
21. http://www.epa.gov/ttn/atw/hlthef/toluene.html.
22. http://www.epa.gov/ttnatw01/hlthef/ethylben.html.
23. Z. C. Hu, S. Pramanik, K. Tan, C. Zheng, W. Liu, X. Zhang, Y. J. Chabal and J. Li, *Cryst. Growth Des.*, 2013, **13**, 4204-07.
24. http://www.chemicalbook.com/ChemicalProductProperty_EN.aspx.
25. http://chem.sis.nlm.nih.gov/chemidplus/jsp/common/PhysicalProperties.jsp.
26. *Handbook Series in Organic Electrochemistry*, CRC Press, 2007.
27. http://www.microkat.gr/msdspd90-99/1-Nitropropane.htm.
28. J. C. Sanchez and W. C. Trogler, *J. Mat. Chem.*, 2008, **18**, 3143-56.
29. M. Uchimiya, L. Gorb, O. Isayev, M. M. Qasim and J. Leszczynski, *Environ Pollut*, 2010, **158**, 3048-53.
30. Y. Liu, R. C. Mills, J. M. Boncella and K. S. Schanze, *Langmuir*, 2001, **17**, 7452-55.
31. H. Sohn, M. J. Sailor, D. Magde and W. C. Trogler, *J. Am. Chem. Soc.*, 2003, **125**, 3821-30.
32. M. E. Germain, T. R. Vargo, P. G. Khalifah and M. J. Knapp, *Inorg. Chem.*, 2007, **46**, 4422-29.
33. B. L. Chen, S. C. Xiang and G. D. Qian, *Acc. Chem. Res.*, 2010, **43**, 1115-24.
34. Y. J. Cui, Y. F. Yue, G. D. Qian and B. L. Chen, *Chem. Rev.*, 2012, **112**, 1126-62.
35. J. R. Li, J. Sculley and H. C. Zhou, *Chem. Rev.*, 2012, **112**, 869-932.
36. M. O'Keeffe and O. M. Yaghi, *Chem. Rev.*, 2012, **112**, 675-702.
37. N. Stock and S. Biswas, *Chem. Rev.*, 2012, **112**, 933-69.
38. M. P. Suh, H. J. Park, T. K. Prasad and D. W. Lim, *Chem. Rev.*, 2012, **112**, 782-835.
39. K. Sumida, D. L. Rogow, J. A. Mason, T. M. McDonald, E. D. Bloch, Z. R. Herm, T. H. Bae and J. R. Long, *Chem. Rev.*, 2012, **112**, 724-81.
40. H. H. Wu, Q. H. Gong, D. H. Olson and J. Li, *Chem. Rev.*, 2012, **112**, 836-68.

41. M. Yoon, R. Srirambalaji and K. Kim, *Chem. Rev.*, 2012, **112**, 1196-231.
42. H. C. Zhou, J. R. Long and O. M. Yaghi, *Chem. Rev.*, 2012, **112**, 673-74.
43. Z. Hu, B. J. Deibert and J. Li, *Chem. Soc. Rev.*, 2014.
44. C. Janiak, *Dalton Trans.*, 2003, 2781-804.
45. L. E. Kreno, K. Leong, O. K. Farha, M. Allendorf, R. P. Van Duyne and J. T. Hupp, *Chem. Rev.*, 2012, **112**, 1105-25.
46. J. C. Sanchez, S. A. Urbas, S. J. Toal, A. G. DiPasquale, A. L. Rheingold and W. C. Trogler, *Macromolecules*, 2008, **41**, 1237-45.
47. L. Pan, H. M. Liu, X. G. Lei, X. Y. Huang, D. H. Olson, N. J. Turro and J. Li, *Angew. Chem. Int. Ed.*, 2003, **42**, 542-+.
48. L. Pan, H. M. Liu, S. P. Kelly, X. Y. Huang, D. H. Olson and J. Li, *Chem. Comm.*, 2003, 854-55.
49. H. Liu, Y. G. Zhao, Z. J. Zhang, N. Nijem, Y. J. Chabal, X. F. Peng, H. P. Zeng and J. Li, *Chem-Asian J*, 2013, **8**, 778-85.
50. J. M. Zhang, H. H. Wu, T. J. Emge and J. Li, *Chem. Comm.*, 2010, **46**, 9152-54.
51. D. Banerjee, Z. C. Hu, S. Pramanik, X. Zhang, H. Wang and J. Li, *Crystengcomm*, 2013, **15**, 9745-50.
52. S. Pramanik, Z. C. Hu, X. Zhang, C. Zheng, S. Kelly and J. Li, *Chem. Eur. J.*, 2013, **19**, 15964-71.
53. Z. Hu, Zhao, Y., Wang, H., Tan, K., Banerjee, D., Zheng, T. J., Emge, T. J., Gong, Q., Chabal, Y. J., Li, J. , *Submitted*, 2014.
54. A. K. Chaudhari, S. S. Nagarkar, B. Joarder and S. K. Ghosh, *Cryst. Growth Des.*, 2013, **13**, 3716-21.
55. Z. Zhang, S. Xiang, X. Rao, Q. Zheng, F. R. Fronczek, G. Qian and B. Chen, *Chem. Comm.*, 2010, **46**, 7205.
56. C. F. Zhu, W. M. Xuan and Y. Cui, *Dalton Trans.*, 2012, **41**, 3928-32.
57. M. Guo and Z.-M. Sun, *J. Mat. Chem.*, 2012, **22**, 15939-46.
58. S. S. Nagarkar, B. Joarder, A. K. Chaudhari, S. Mukherjee and S. K. Ghosh, *Angew. Chem. Int. Ed.*, 2013, **52**, 2881-85.
59. L. B. Sun, H. Z. Xing, J. Xu, Z. Q. Liang, J. H. Yu and R. R. Xu, *Dalton Trans.*, 2013, **42**, 5508-13.
60. T. K. Kim, J. H. Lee, D. Moon and H. R. Moon, *Inorg. Chem.*, 2013, **52**, 589-95.
61. Y. S. Xue, Y. B. He, L. Zhou, F. J. Chen, Y. Xu, H. B. Du, X. Z. You and B. L. Chen, *J. Mat. Chem. A.*, 2013, **1**, 4525-30.
62. S. K. Nune, P. K. Thallapally and B. P. McGrail, *J. Mat. Chem.*, 2010, **20**, 7623-25.
63. D. Zhao and T. M. Swager, *Macromolecules*, 2005, **38**, 9377-84.
64. S. Barman, J. A. Garg, O. Blacque, K. Venkatesan and H. Berke, *Chem. Comm.*, 2012, **48**, 11127-29.
65. X. H. Zhou, H. H. Li, H. P. Xiao, L. Li, Q. Zhao, T. Yang, J. L. Zuo and W. Huang, *Dalton Trans.*, 2013, **42**, 5718-23.
66. X. H. Zhou, L. Li, H. H. Li, A. Li, T. Yang and W. Huang, *Dalton Trans.*, 2013, **42**, 12403-09.
67. H. Xu, F. Liu, Y. Cui, B. Chen and G. Qian, *Chem. Comm.*, 2011, **47**, 3153.
68. S.-B. Ding, W. Wang, L.-G. Qiu, Y.-P. Yuan, F.-M. Peng, X. Jiang, A.-J. Xie, Y.-H. Shen and J.-F. Zhu, *Mat. Lett.*, 2011, **65**, 1385-87.
69. C. Y. Zhang, Y. K. Che, Z. X. Zhang, X. M. Yang and L. Zang, *Chem. Comm.*, 2011, **47**, 2336-38.
70. B. Gole, A. K. Bar and P. S. Mukherjee, *Chem. Comm.*, 2011, **47**, 12137.
71. R. Li, Y. P. Yuan, L. G. Qiu, W. Zhang and J. F. Zhu, *Small*, 2012, **8**, 225-30.
72. Q. R. Fang, G. S. Zhu, M. Xue, Z. P. Wang, J. Y. Sun and S. L. Qiu, *Cryst. Growth Des.*, 2008, **8**, 319-29.
73. Y. Y. Long, H. B. Chen, Y. Yang, H. M. Wang, Y. F. Yang, N. Li, K. A. Li, J. Pei and F. Liu, *Macromolecules*, 2009, **42**, 6501-09.
74. Y. P. Wang, F. Wang, D. F. Luo, L. Zhou and L. L. Wen, *Inorg. Chem. Comm.*, 2012, **19**, 43-46.
75. Y. P. Yuan, W. Wang, L. G. Qiu, F. M. Peng, X. Jiang, A. J. Xie, Y. H. Shen, X. Y. Tian and L. D. Zhang, *Mater. Chem. Phys.*, 2011, **131**, 358-61.
76. K. L. Zhang, H. Y. Gao, N. Qiao, F. Zhou and G. W. Diao, *Inorg Chim Acta*, 2008, **361**, 153-60.
77. A. Thirumurugan and C. N. R. Rao, *J. Mat. Chem.*, 2005, **15**, 3852-58.
78. L. N. Li, S. Q. Zhang, L. J. Xu, L. Han, Z. N. Chen and J. H. Luo, *Inorg. Chem.*, 2013, **52**, 12323-25.
79. S. Zhang, L. Han, L. Li, J. Cheng, D. Yuan and J. Luo, *Cryst. Growth Des.*, 2013, **13**, 5466-72.
80. R. Xiong, J. T. Fern, D. J. Keffer, M. Fuentes-Cabrera and D. M. Nicholson, *Mol. Simulat.*, 2009, **35**, 910-19.
81. R. Xiong, D. J. Keffer, M. Fuentes-Cabrera, D. M. Nicholson, A. Michalkova, T. Petrova, J. Leszczynski, K. Odbadrakh, B. L. Doss and J. P. Lewis, *Langmuir*, 2010, **26**, 5942-50.
82. R. Xiong, K. Odbadrakh, A. Michalkova, J. P. Luna, T. Petrova, D. J. Keffer, D. M. Nicholson, M. A. Fuentes-Cabrera, J. P. Lewis and J. Leszczynski, *Sensor Actuat. B-Chem.*, 2010, **148**, 459-68.
83. J. D. Xiao, L. G. Qiu, F. Ke, Y. P. Yuan, G. S. Xu, Y. M. Wang and X. Jiang, *J. Mat. Chem. A.*, 2013, **1**, 8745-52.
84. B. D. Wagner, G. J. McManus, B. Moulton and M. J. Zaworotko, *Chem. Comm.*, 2002, 2176-77.
85. E. Y. Lee, S. Y. Jang and M. P. Suh, *J. Am. Chem. Soc.*, 2005, **127**, 6374-81.
86. D. Maspoch, D. Ruiz-Molina and J. Veciana, *Chem. Soc. Rev.*, 2007, **36**, 770-818.

TOC

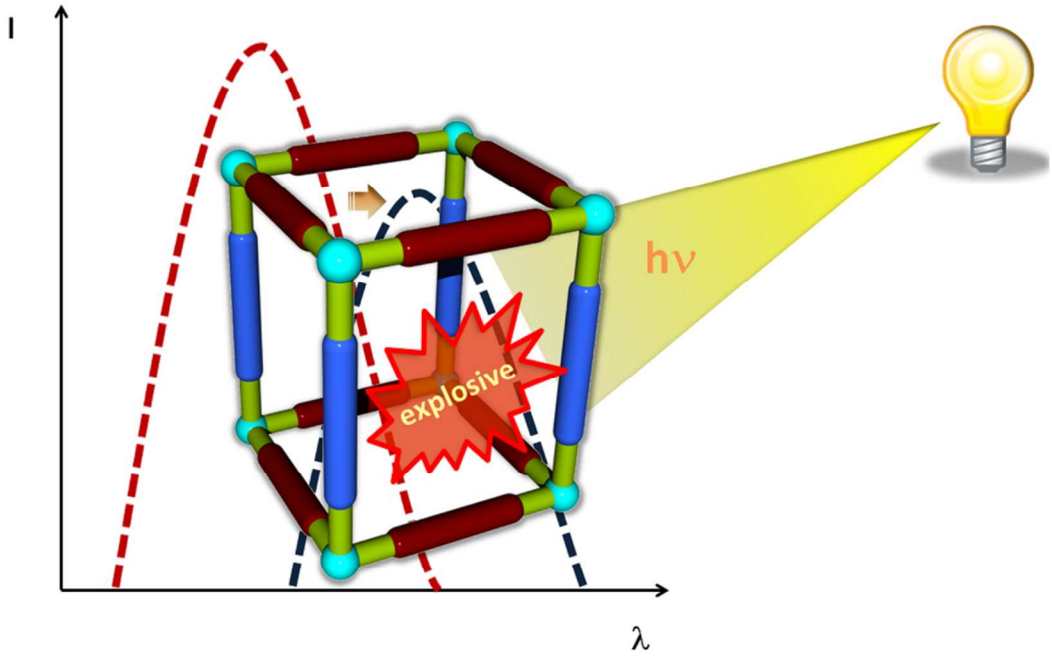

A perspective summarizing the recent advancement on explosive sensing by luminescent metal organic framework (LMOF) materials.